BACHELOR

Spectral and temporal investigation of lasing operation in photonic crystal nanocavities

Koolen, R.

Award date:
2018

Technische Universiteit Eindhoven University of Technology

Applied Physics

Bachelor End Project

Photonics and Semiconductor Nanophysics

Quartile 4: 2017-2018

Spectral and temporal investigation of lasing operation in photonic crystal nanocavities

R. Koolen 0949001
Daniele Pellegrino MSc. supervisor

Eindhoven, July 3, 2018

Abstract

In this work, photonic crystal cavities (PCCs) including high density self-assembled InAs quantum dots (QDs) are studied in order to observe signatures of lasing operation. More specifically, the QDs emission into the modes of an unmodified L3, and modified L3, L7 and L11 PCC are studied in the spectral and temporal domain by means of a microphotoluminescence (µPL) and time correlated single-photon counting (TCSPC) setups. The fundamental modes of the modified showed behavior reminiscent of lasing thresholds at 1.3µW to 3.0 µW, 26.2 µW to 35.8µW and 19.6µW to 22.1µW for the L3/7/11 cavities respectively. The lasing devices show a strong power dependent decay rate that can be used as signature for lasing. From this work, it can be concluded that modifiied designs of L3, L7 and L11 PCC are good candidates of lasing as they show signatures of lasing operation. During the study a lineshape with a non-Lorentzian feature presented itself at lasing conditions. This feature could have a relation to lasing, however this requires further investigation. Furthermore, additional investigation of the second-order correlation function $g^{(2)}(0)$ is needed to unambiguously prove lasing.

Contents

1 Introduction

Lasers are a widely used tool in many applications ranging from medicine[1] to communication[2]. This is due to their highly tunable properties such as power, emission range and pulse duration. Currently a popular area of study is the investigation whether microscopic devices which currently operate on electricity, such as integrated circuits, can also operate on light[3]. Decreasing the size of these lasers to the nanometer size allows them to be integrated into microscopic devices, opening up a new world of optically operated devices.

Quantum Dots (QDs) embedded in Photonic Crystal Cavities (PCC) represent a scalable way of fabrication nanolasers due to the easy integration of the QDs into complex photonic structures[4]. PCC show profound Purcell enhanced (PE) spontaneous emission (SE)[5][6]. Near thresholdless lasing is possible due to the high SE rate ratio into the lasing mode[7]. Furthermore these lasers exhibit lasing thresholds orders of magnitude lower than conventional VCSEL lasers[8][9]. Not only do these PE enhanced nanolasers have low thresholds, they are very efficient[10] and have high modulation speeds[11][12]. These PE enhanced PCC nanolasers present possible device applications in optical communication[13], on-chip interconnects[14], biochemical sensing[15] and quantum information processing[16].

This work is part of a larger project which aims to control the radiative interaction between InAs QDs and one of three coupled nanocavities[17]. By non-locally moulding the mode field experienced by the QDs inside one of the cavities, it is possible to deterministically tune, and even inhibit, the spontaneous emission into the cavity mode. These nanocavities are investigated for lasing as this tuning mechanism could allow for ultrafast non-local modulation of laser pulses. Nanocavities which are able to efficiently emit ultrafast laserpulses show great promise for applications in high-speed communications[13], information processing[18] and on-chip optical interconnects[14].

In this report, an experimental study for lasing in PCC using QDs as gain medium is presented. More specifically, modified L3, L7 and L11 PCCs containing self-assembled QDs are investigated in the spectral and temporal domain by means of microphotoluminescence (µPL) and time correlated single-photon counting (TCSPC) setups. The structure of this report is the following: Section 2 presents the background information necessary for investigation lasing in PCC. Section 3 elaborates on the experimental method used to obtain this evidence. Section 4 presents the results of a characterization study on the PCC after which Section 5 presents the results obtained by the spectral measurements. Section 6 explores the influence of the leaky modes in the L-L curves. Section 7 illustrates the presence of a non-Lorentzian feature in the cavity mode and its dependencies. Afterwards Section 8 present the results of the time resolved µPL measurements on the PCC. Subsequently, Section 9 discusses upon the results obtained during this study. Finally, the conclusions of this report are given in Section 10

2 Theory

2.1 Photonic crystals

Photonic crystals are the optical analogue to semiconductors. The periodic potential which affects the motion of electrons in semiconductors is replaced by a periodic dielectric function. Such a periodic function modifies the propagation of photons within the photonic crystal which result in the creation of a band gap. This band gap can effectively block light propagation with specific frequencies in certain directions. For example, in its most general sense, a distributed Bragg mirror is a 1D photonic crystal.

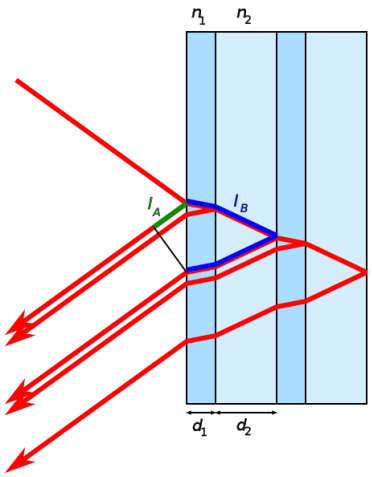

Figure 2.1: *Diagram of a 1D Bragg mirror. Thin layers with a high refractive index n1 are interleaved with thicker layers with a lower refractive index n2. The path lengths l_A and l_B differ by exactly one wavelength, which leads to constructive interference.*

Fig. 2.1 provides a schematic as to how a 1D Bragg mirror operates. The interference occurring after the reflection at each boundary prevents certain wavelengths from propagating inside the crystal, therefore creating a photonic crystal band gap.

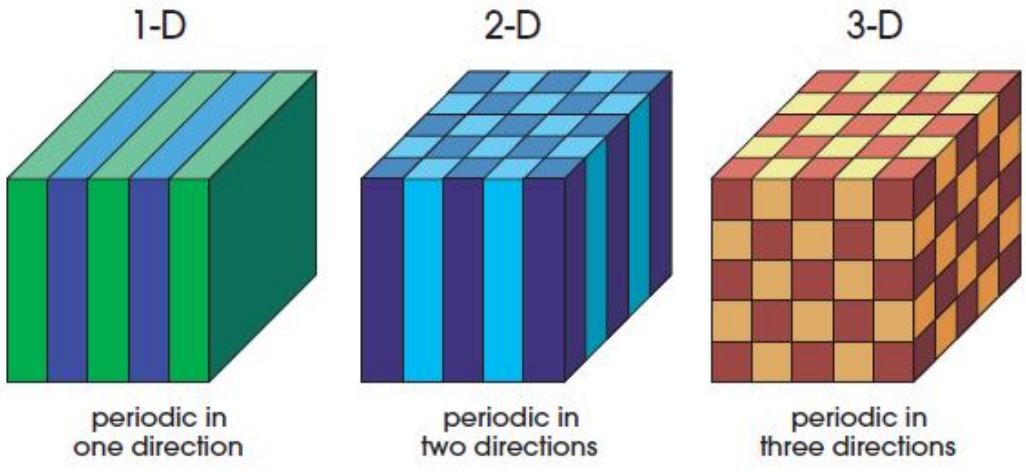

Figure 2.2: *Simple examples of one-,two- and three-dimensional photonic crystals. The different colors represent materials with different dielectric constants. The defining feature of a photonic crystal is the periodicity of dielectric material along one or more axes.[19]*

The concept of a photonic crystal can be extended into higher dimensionality. In this case instead of an alternating dielectric constant in one direction, there is an periodicity in the dielectric constant in two or three directions. A schematic of this is depicted in Fig. 2.2. The extension of the alternating dielectric

into additional dimensions also introduces a photonic band gap in said dimensions.

2.1.1 Photonic bandgap

The reason as to why the photonic band gaps appear lies within the fact that according to the electromagnetic variational theorem[19], low frequency modes concentrate their energy in high-ϵ regions, where ϵ is the dielectric constant of the material, and the high frequency modes have a larger fraction of their energy present in low-ϵ modes. An example of this is shown in Fig. 2.3.

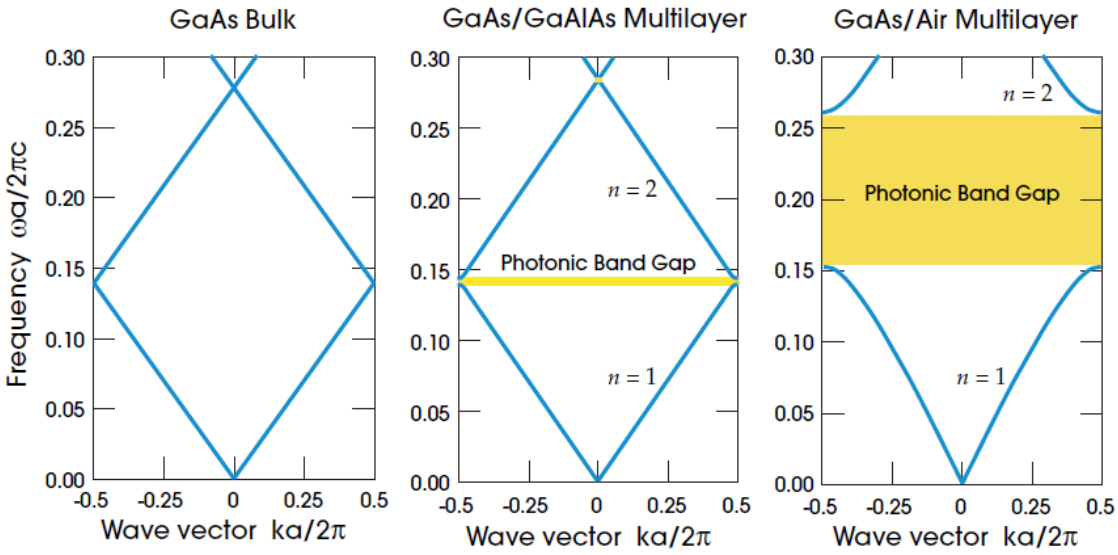

Figure 2.3: *Photonic band structures for in-axis propagation. For all three cases the layer has a width of 0.5A, where A is the lattice constant. Left: every layer has the same dielectric constant epsilon=13. Middle: the layers have alternating dielectric constants of ϵ=13 and ϵ=12. Right: the layers have alternating dielectric constants of ϵ=13 and ϵ=1[19].*

This explains why there is a frequency difference between the two cases (n=1 and n=2). The mode which lies below the band gap has its energy concentrated in the higher ϵ region which results in a lower frequency and vice versa. In Fig 2.3, the width of the photonic crystal band gap depends on the dielectric constant mismatch between the materials compsoing the photonic crystal.

2.1.2 Photonic crystal slabs

Photonic crystal slabs are photonic crystals with a two dimensional periodicity and with a finite thickness. While these hybrid structures may seem two dimensional, since they have a finite thickness they are not the same as 2D photonic crystals. The finite thickness introduces new behavior in the vertical dimension. The light will experience guided propagation if the wavevector lies outside the bandgap as there are now allowed modes within this gap. The light will escape the slab if the wavevector lies within the light cone.

Usually two kinds of photonic crystal slabs are considered. A square lattice of dielectric rods in air and a triangular lattice of air holes in dielectric. An example of this is shown in Figure 2.4. These are referred to as rod slabs and hole slabs.

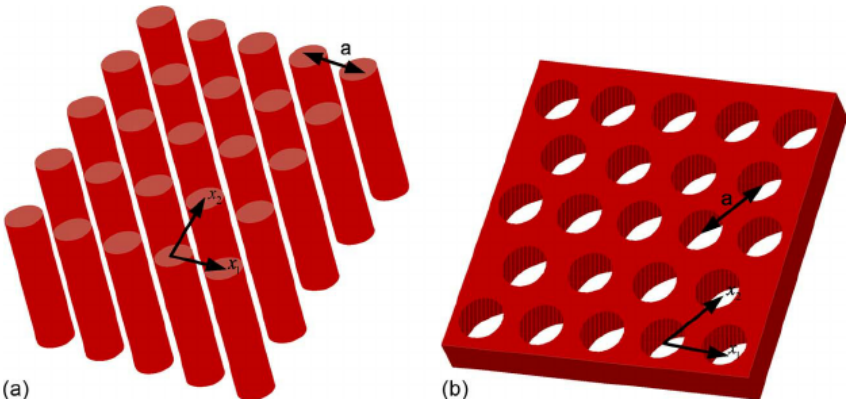

Figure 2.4: *(a)Photonic crystal slabs. Square lattice of rods in air (rod slab).(b)Triangular lattice of holes in a dielectric slab (hole slab).[20]*

With discrete translational symmetry of the crystal in the x and y direction the in plane wave vector is conserved. However because of the finite thickness the vertical vector is generally not conserved. In work a hole slab(made of GaAs) is considered

2.2 Photonic crystal cavities

Similar to semiconductors where certain desirable properties can be achieved by introducing certain defects, for example by P or N doping, certain properties can be introduced into photonic crystals by introducing defects as well. For example by introducing a linear defect is is possible to create a mode which is inside the band gap. A different application of introducing defects by removing holes or rods is the photonic crystal cavity(PCC) also known as a nanophotonic resonator. This structure has periodic changes in the dielectric constant with a periodicity of the order of the wavelength of the light at IR frequencies. Due to the band gap which arises at the cavity edge, light of certain wavelengths is not allowed to propagate into the crystal in the in-plane direction and is confined to the cavity[21]. The slab boundaries in the out-of-plane-direction can provide another reflection surface due to oblique reflection at dielectric boundaries, this is also known as total internal reflection.

A common designs for a PCC are the linear defect, Lx-type, cavities. Lx refers to a photonic crystal which has x number of holes or rods missing in a linear fashion, creating a resonator. Fig. 2.5 provides an example as to how a L3 cavity looks like.

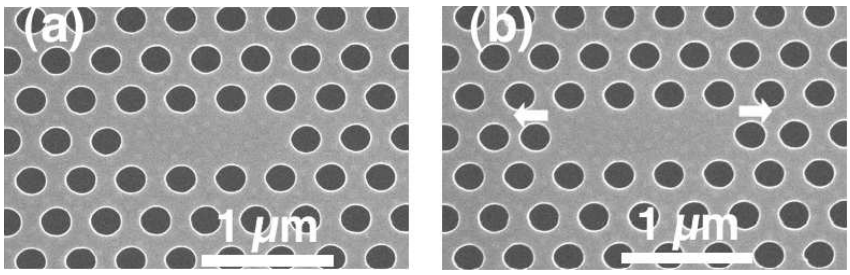

Figure 2.5: *(a) Example of a L3 photonic crystal cavity. As shown there are 3 air holes missing creating a resonator cavity.(b) A similar L3 cavity except the lateral air holes have shifted their position.[22]*

It is possible to optimize the confinement of the light in the cavity by changing certain design parameters. The confinement of the light inside the cavity is quantified with the Quality factor, or Q factor. The Q factor is defined as

$$Q = \frac{\lambda}{\Delta\lambda} \tag{1}$$

where Q is the Q factor, λ is the center of the mode and $\Delta\lambda$ is the corresponding Full Width Half Maximum (FWHM) of the mode. This means that a cavity which has a narrow mode has a high Q factor. Furthermore the photon lifetime inside the cavity is also proportional to the Q factor. This

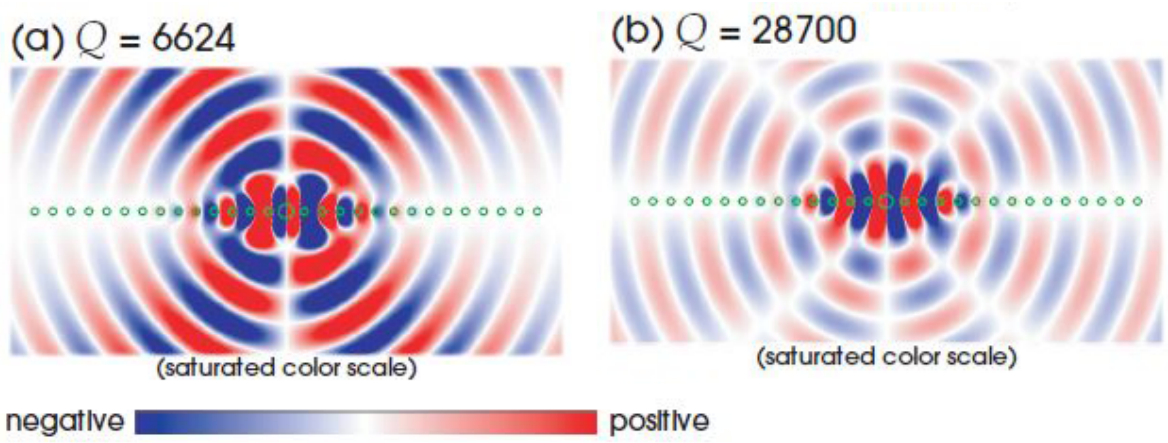

Figure 2.6: *(right) Increase in Q factor due to a cancellation of the lowest order multipole term in the radiative field.(left) A lower Q factor due to the presence of a lower order term in the multipole expansion[19].*

means that a cavity with a high Q factor, hence a high photon lifetime, confines the light better inside the cavity than a cavity with a lower Q factor.
Changing the Q factor can be done by changing various parameters such as the hole radius, the displacement of the lateral edge holes, or reducing the radius of various holes at the cavity boundary[23]. The mechanism usually responsible for changing the Q factor drastically without changing the modal volume is cancellation[19]. The dominant component of the radiation is eliminated by a forced balance of scattered fields with opposite signs. The radiated field can be described by a multipole expansion. It turns out that the radiated field is simply the sum of contribution of each multipole term, i.e. there is no inter-term interference. If cavity can be modified in such a way that the dominant term in the scattered field (usually the dipole term) vanishes, the Q factor will greatly be enhanced. This also results in that the far field will take on characteristics of a higher-order radiation pattern.

Fig. 2.6 shows the radiative field of two cavities. A clear difference in the far field is visible. The right image shows more modes in the far field than the right image. This is due to cancellation of the lowest-order multipole term and results in a higher Q factor.

The design parameters used in this study are elaborated on in Section 3.2.

2.3 Quantum dots

Quantum dots are semiconductor nanostructures with sizes typically in the order of several nanometers. The reason quantum dots show interesting behavior is that when a devices size is reduced to a characteristic size, quantization effects take place. In the case of quantum dots if the carrier motion is limited to a distance in the order of the carrier de Broglie wavelength, quantization effects will occur. The de Broglie wavelength is given by the following relation:

$$\lambda = \frac{h}{p} = \frac{h}{\sqrt{3m_{eff}kT}} \tag{2}$$

where λ is the de Broglie wavelength, h is Planck's constant, p the momentum of the carrier, m_{eff} the effective mass of the particle, k Boltzmann's constant and T the temperature.

When the infinite extension in all three dimensions of a device gets reduced to several nanometers, carrier localization in all three dimensions takes place and the classical band structure model of a continuous energy dispersion relationship breaks down. The resulting density of states (DOS) of quantum dots is discrete as shown in Fig. 2.7.

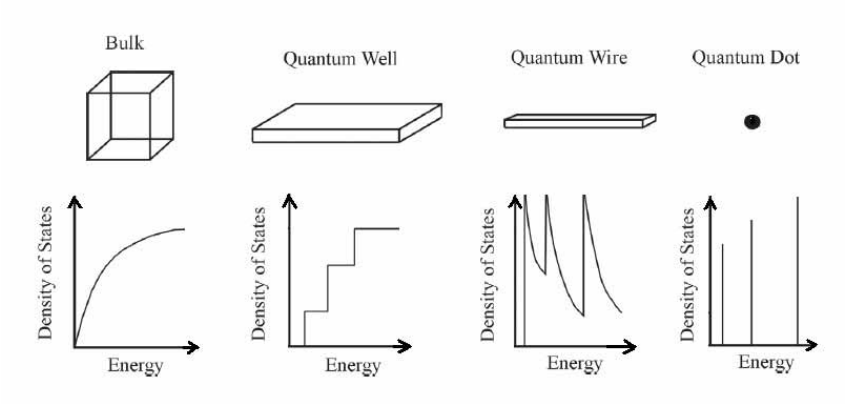

Figure 2.7: *The density of states(DOS) is shown as function of energy for several material shapes. Quantum Dots(right) show a discrete DOS[24].*

This discretization of DOS results in narrow emission spectra of quantum dots. This narrow emission spectrum can be affected by temperature related homogeneous broadening[25] or inhomogeneous broadening. Inhomogenous broadening is the result by lack of control of the QD size dimensions during the manufacturing process as their emission wavelength is dependent on their size.

One method of creating QDs is by self assembly. Stranksi and Krastanow proposed a method of of island formation on an initially flat heteroepitaxial surface. This process is known as Stranksi Krastanow growth (SK growth)[26].
The process generally consists out of the following steps. Initially complete films of adsorbates, which can be up to several monolayers thick, grow in a layer-by-layer fashion on a substrate. Beyond a critical layer thickness, which depends on strain and the chemical potential of the deposited film, growth continues through the nucleation and coalescence of adsorbate islands[27]. These island then are able to grow to dimension desirable for the QDs in question.

2.4 Lasers

2.4.1 Introduction lasers

A laser is a device which emits light through a process based on optical amplification by stimulated emission. The term laser originated as an acronym for "light amplification by stimulated emission of radiation". A laser differs from normal (thermal) light sources by the fact that it is a source of spatially and temporally coherent light.

A laser consists out of a gain medium, a power source to provide power to the gain medium, also known as a pump, and something to provide optical feedback (i.e. an optical resonator)[28]. How these components relate to each other in a laser are described by the laser rate equations. A general derivation of these equations can be found in Appendix A. However a different way to describe the laser rate equations, which is possibly better suited for nanolasers, is a derivation based in Fermi's golden rule as this derivation does not rely on ad hoc introduction of parameters such as the spontaneous emission factor β [29].
In this experiment the gain medium are self assembled QDs, the power source is a pulsed excitation laser and the optical feedback is provided by a PCC. This will be further elaborated on in Section 3.

As mentioned above, the light emitted by a laser is spatially and temporally coherent. However this is not always the case. Lasers only emit coherent light above a certain threshold, called the lasing threshold. One of the definitions of the lasing threshold is that it is the lowest excitation level where the output is dominated by stimulated emission rather than by spontaneous emission. This is characterized by a nonlinearity in the pump power vs output power curve also known as a L-L curve. However, this definition is not always applicable as is the case for nanolasers. The most general definition of the lasing threshold is the point where the gain equals the loss of the optical resonator. Besides the transition of incoherent emission to coherent emission there are various indicators of lasing. These signatures will be elaborated on in Section 2.4.2.

2.4.2 Signatures of lasing

Lasers operate in the weak coupling regime. Weak coupling corresponds to a regime which can be described using perturbation theory and the spontaneous emission (SE) rate can be determined with Fermi's golden rule. In conventional lasers whose cavity dimensions are much larger than the light wavelength, the free spectral range of the cavity modes is small and a large number of modes interacts with the active material. Consequently a large number of SE modes from the active material is coupled into nonlasing modes. The ratio of the SE coupled into the lasing mode divided by all modes is called the spontaneous emission factor β.

For conventional lasers, where β is relatively low, the transition from SE regime (below threshold) to the lasing regime (above threshold) can be characterized by some of the following key features:

- Observation of nonlinearity in the output power at lasing threshold.
- Schawlow-Townes linewidth narrowing of the cavity mode.
- Transition from from 2 to 1 in the second order correlation function at zero delay $g^{(2)}(\tau = 0)$ which corresponds with a change in the probability of two photon coincidence.
- Decrease of the carrier lifetime.

It is important to note that these are not independent criteria. Changes in the output power or emission intensity, coherence properties and two photon coincidence all are related to the underlying photon statistics.

Sharp increase output power

For conventional lasers the main indicator of a lasing threshold is the sharp increase of output power. This sudden increase can be as big as several orders of magnitude and is easily detectable in the case of conventional lasers. According to a rate equation analysis of Yokoyama and Brorson the intensity jump at the threshold scales with $1/\beta$[30]. This means that in the case where β approaches unity, which means that all the emission is funneled into the lasing mode, the threshold starts to disappear as is shown in Figure 2.8. A β approaching one can be realized with a cavity which has a high Q factor and low mode volume where the emission into the lasing mode is enhanced and the emission into the nonlasing modes is zero. It has been demonstrated that for 3D photon confinement with Q factors over 10^4 and a mode

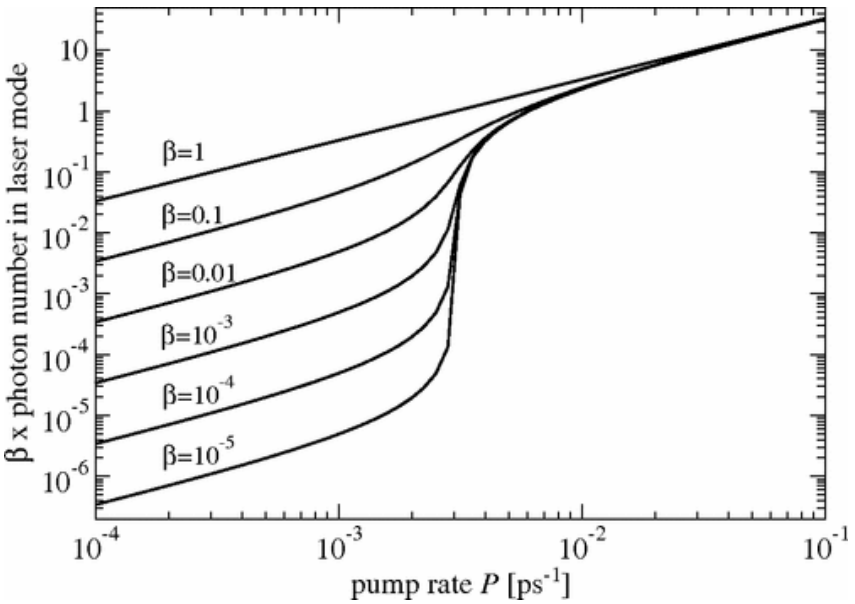

Figure 2.8: *L-L curve of a laser for various β factors obtained by numerical simulations based on semiconductor theory originating from a microscopic Hamiltonian to describe lasing from quantum dots embedded in microcavities. A cavity lifetime of 17ps for and a spontaneous emission lifetime of 50ps have been used[31].*

volume approaching the cubic of the light wavelength, the laser threshold in the L-L curve becomes difficult to observe[32][10]. Furthermore, care must be taken when using the sudden increase in output power as evidence for QD lasing as several QD configurations such as exciton or biexciton can contribute to nonlinearities in the L-L curve. For example a sudden increase in the L-L can also occur when the biexcition contribution takes over at higher excitation power and the excition contribution saturates[33]. Thus in order to determine whether a nanolaser is lasing, it is important to consider the other features which indicate stimulated emission.

Linewidth narrowing

As mentioned in 2.4.2, a different signature of lasing is the linewidth narrowing of the lasing mode. For a conventional laser the linewidth varies inversely with the output power or photon density according to the Schawlow-Townes limit[34]. For conventional lasers the Schawlow-Townes equation is the following:

$$\Delta\nu_{ST} = \frac{\Gamma R_{SE}}{4\pi n_\phi} \tag{3}$$

At threshold the photon density, n_ϕ shows a drastic increase as shown in 2.8, therefore according to equation 3 the linewidth should show a sudden narrowing as well. However small mode volume semiconductor, high β, lasers stay well above the Schawlow-Townes limit[35] the strongly increase SE rate into the lasing mode can no longer be described as a small perturbat For a VCSEL with a QW gain medium it was observed that a pronounced plateauing of the linewidth appears around the lasing threshold regime[36]. In this case the reason for the plateauing lies within the coupling between intensity and phase noise which is rather important in semiconductor lasers which have a QW gain.

L3 type QD nanolasers display a similar plateau in the linewidth narrowing as fuction of power, however, at a reduced magnitude as shown in Figure 2.9. Alternatively a L3 type QD nanolaser with a different design only shows a monotonous decrease in linewidth indicating that this device is not lasing. As men-

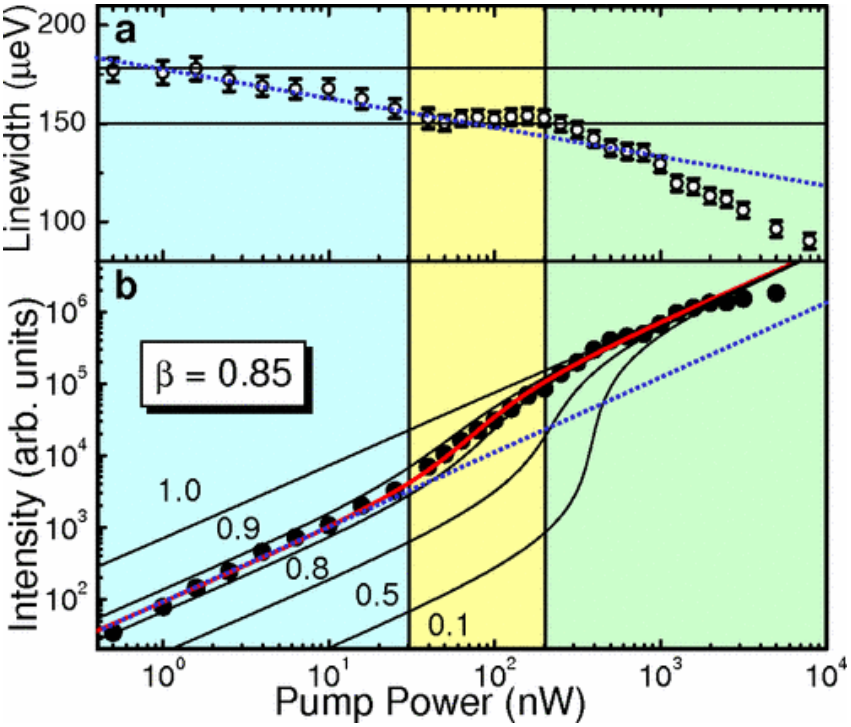

Figure 2.9: *(a) linewidth narrowing and (b) L-L curve for a L3 type photonic crystal nanolaser with a QD density of 8 QD's per μm^2 (solid dots). The dotted blue lines indicate the measured data for nonlasing devices on the same wafer[37].*

tioned in 2.4.2 the sudden kink in output power itself should not necessarily be an indication of lasing. However as is shown in Figure 2.9 the kink in output power corresponds with a plateauing of the lasing mode linewidth indicating a lasing threshold.

$g^{(2)}(0)$ decrease

The second order correlation function or intensity autocorrelation function measures the correlation of intensities of two incident paths at a certain delay τ. It is defined in the following manner:

$$g^{(2)}(t,\tau) = \frac{\langle b^\dagger(t)b^\dagger(t+\tau)b(t+\tau)b(t)\rangle}{\langle b^\dagger(t)b(t)\rangle\langle b^\dagger(t+\tau)b(t+\tau)\rangle} \tag{4}$$

where $b^\dagger$ and b are the photon creation and annihilation operators for the lasing mode. For the special case of $\tau = 0$, the second order correlation function analyzes the two photon incidence. In a stationary situation the second order correlation function does not depend on t and the $g^{(2)}(0)$ becomes an indicator of certain characteristic properties of the underlying photon statistics of the emitter.

Consequently a different signature of lasing is the transition of the intensity autocorrelation function $g^{(2)}(0)$ from 2(thermal light) to 1(coherent light). For a conventional laser the $g^{(2)}(0)$ has a sharp transition from 2 to 1 at the lasing threshold. In the case of nanolasers with high β this transition becomes more gradual and for the case of β =1 a large transition area appears.

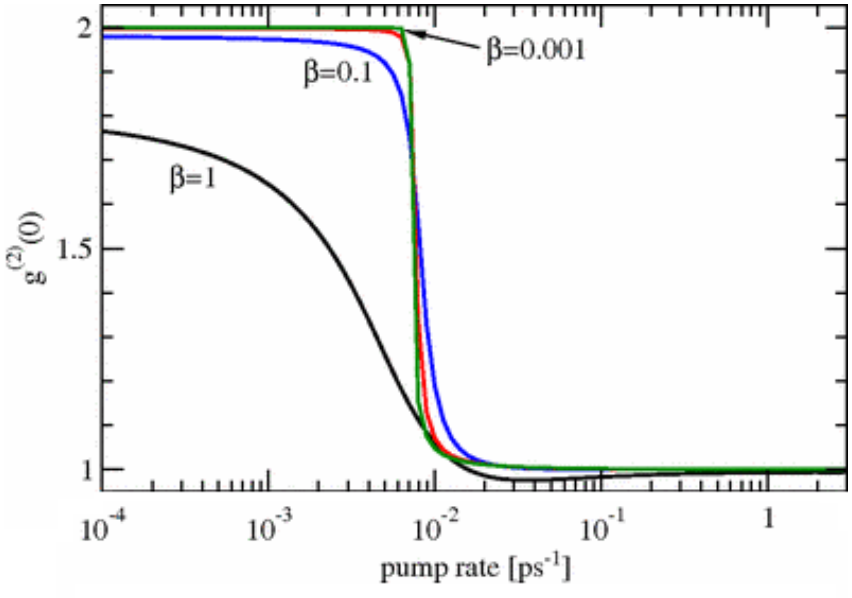

Figure 2.10: *The $g^{(2)}(0)$ calculated for various β by the same model as was used in Figure 2.8[31].*

As is shown in Figure 2.10 the transition for high β lasers is rather broad. However even in this case above threshold the value of the $g^{(2)}(0)$ becomes 1 indicating coherent emission which indicates the lasing operation.

Carrier lifetime decrease

In general the carrier lifetime of the active material in a cavity is a function of the carrier density n in the material. This is best understood by looking at the gain and carrier clamping mechanism of conventional lasers as shown in Figure 2.11. The steady state gain,g, in a laser operating above threshold must be equal to its threshold value, g_{th}. Were this not the case, the field amplitude would increase without bound which is clearly nonphysical.
Furthermore because the gain has a linear relationship to the carrier density, the carrier density must also clamp at its threshold value[38]. This means that when even more carriers get introduced, while at the lasing threshold, in the active region, the carrier lifetime must decrease in order to reach a new steady state[38]. This process results in a new steady-state where the threshold requirements are satisfied again. While the clamping is less pronounced for lasers with high β a sudden carrier lifetime reduction is still indicative of the presence of a lasing threshold.

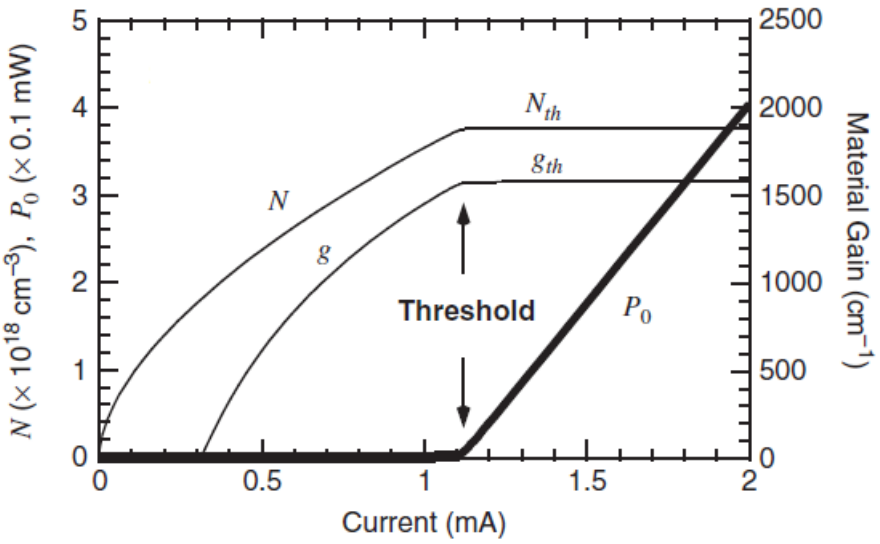

Figure 2.11: *Output power P_0 versus current for an in plane laser. The carrier density, N, and material gain, g, as function of current are shown as well[28]. At the lasing threshold the gain and carrier density clamp at their threshold values g_{th} and N_{th} respectively.*

The carrier lifetime can be quantified by solving the carrier rate equation which is given in equation A.6 for a cavity which has no pump power, meaning no carrier generation. Solving this equation gives:

$$n(t) = n(0)e^{\frac{-t}{\tau}} \tag{5}$$

Where $n(t)$ is the carrier density at t and $n(0)$ is the carrier density at t=0. Therefore the carrier density should show an exponential decay in the absence of any excitation power.

3 Experimental Method

3.1 Setup description

During the course of this project several spectral and time resolved measurements were made with a microphotoluminesence (µPL) setup.

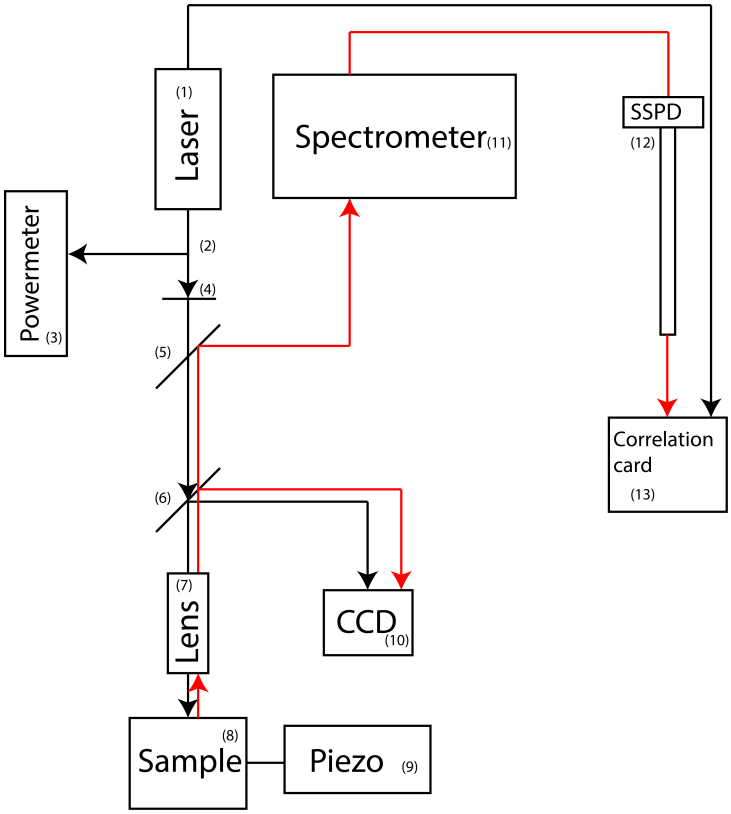

Figure 3.1: *Schematic drawing of the setup. Black arrow indicates light which originates from the excitation laser, the red arrow indicates emitted from the QDs.*

The setup is schematically illustrated in Fig. 3.1 where the important parts are numbered from (1) to (13).

3.1.1 Spectral measurements

For the spectral resolved measurements, the parts from (1) to (11) were used. The excitation laser(1) in this experiment is a PicoHarp PDL 800-B (750 nm, Max repetition rate 80Mhz) pulsed laser. This laser provides the pump power to excite the quantum dots in the sample(8). The fiber is then coupled into a 50/50 fiber beamsplitter which splits the light into two fibers. One fiber is connected to a power meter(3) and the other fiber is connected to a fiber optic collimator with lens(4) that couples the light into free space, which defines the µPL principal axis. The excitation power is changed using a fiber optic attenuator.

At the optical table the excitation beam passes through a dichroic mirror(cutoff wavelength 1000 nm)(5). As the wavelength of the excitation beam lies below the cutoff wavelength it does not get reflected. Following the dichroic mirror is a 8/92 beamsplitter where 8% of the light is reflected towards a CCD(10) and 92% is transmitted towards a 100x focus lens(7) which focuses the light on the the sample(8). The sample can be moved in the in-plane-directions (x and y) by a piezo element(9). This allows the sample to be placed in such a way that the excitation beam hits the sample in a spot where a cavity is positioned. The piezo also allows movement in the z-direction. This allows for the sample to be placed at the focal point of the excitation beam, optimizing the pump power into the cavity. The sample contains QDs in a PCC which are excited by the excitation beam. The sample can be cooled down, using liquid

nitrogen, to 77K. More details on the sample are provided in Section 3.2. The light emitted by the sample (indicated by the *red* arrow) then reaches the same 8/92 beamsplitter(6). A part of the light is directed towards the CCD which allows the experimenter to see the position of the spot on the sample. The majority of the light passes through and gets reflected by the dichroic mirror(5). After the reflection by the dichroic mirror, the light is directed towards a spectrometer(11)(Horiba iHR1000) which analyzes the light emitted by the sample. The spectrometer can take spectra with low or high resolution grating. The high resolution grating has a resolution of 0.02 nm and the low resolution grating has a resolution of 0.08 nm. The low resolution grating will not be used intensively as it provides resolution limited results in most cases. Hence the spectra which will provide the data in this experiment will be taken with the high resolution grating.

3.1.2 Time resolved measurements

In order to measure the QDs their decay time, time resolved measurements were performed. The setup which is used for the spectral measurements is used as well for the time resolved measurements (parts (1)to (11)). In order to perform these measurements the spectrometer is used as a spectral filter. A single grating is opened in the spectrometer functioning as a bandpass with a width of 0.1 nm. The incoming light is then detected by a Superconducting Single Photon Detector (SSPD)(12). This detector is cooled to 1.6K by liquid helium. The SSPD is connected to a PicoHarp 300 correlation card (13). The PicoHarp 300 has two independent, but synchronized, input channels. This allows the PicoHardp 300 to use them as start and stop signals for Time Correlated Single Photon Counting (TCSPC). In this case the PicoHarp 800 PDL800-B laser integrated trigger is used as start signal, while the signal from the SSPD is used as stop signal. The time passed between the start and stop signals are recorded and using these values a histogram is created. From this histogram, the dynamics of the QDs can be reconstructed. The instrument response function (IRF) of this measurement gives a time resolution of 75 ps.

3.2 Sample

The sample used during the experiment contains L3/7/11 photonic crystal cavities consisting of a 220 nm thick GaAs membrane with one layer of self assembled QDs. The QD's have an areal density of 200 QD's/μm^2 and have a ground state emission at 1230 nm at 77 K as shown in Fig. C.1. The QD's were assembled using the Stranski Krastanow method and are embedded in the center of the cavity. The fabrication of the sample, provided by nanoPHAB, involves dry etching holes on a GaAs membrane with a 1.5 µm sacrificial layer of $Al_{0.7}Ga_{0.3}As$.

Figure 3.2 shows a SEM image of an unmodified L3 cavity. The absence of air holes in the center, creating a cavity, is clearly visible in the SEM.

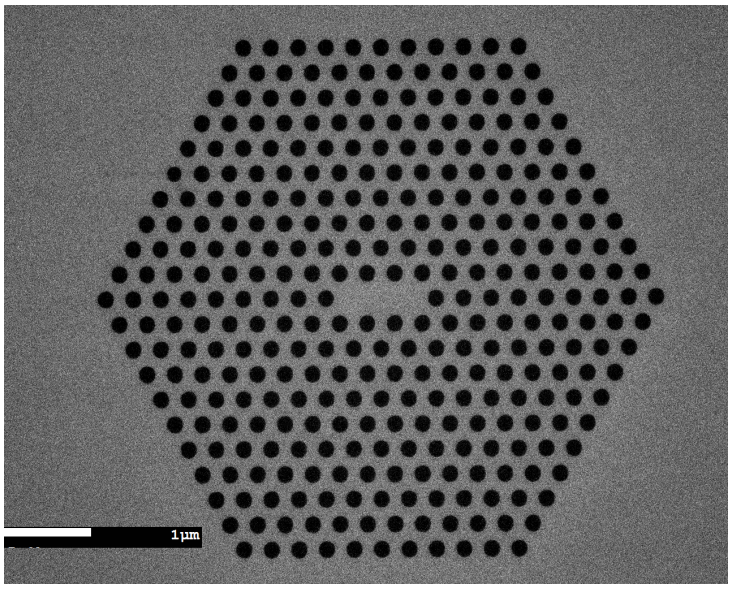

Figure 3.2: *SEM image of an unmodified L3 cavity. Courtesy of F. Pagliano*

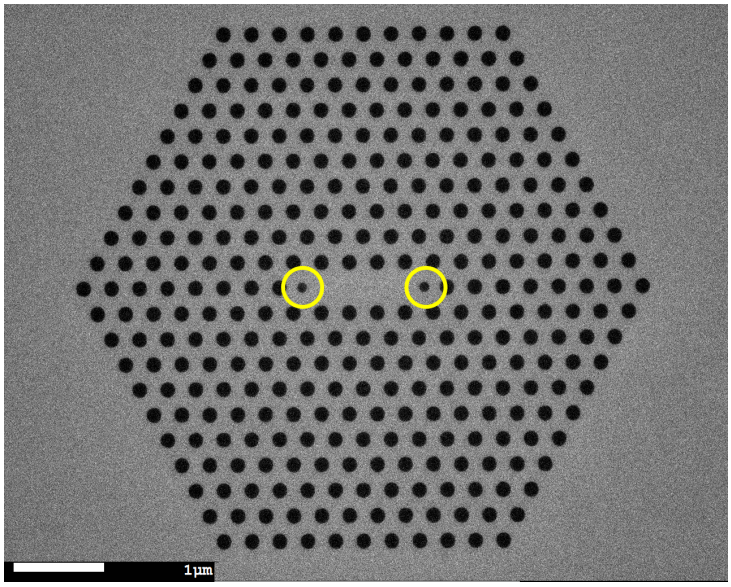

Figure 3.3: *SEM image of a modified L3 cavity. The yellow circles indicate the modified air holes. The air hole modifications are RM70 and S016. Courtesy of F. Pagliano*

The sample contains PCC which are characterized by the following parameters:

- Lx, where x is referring to the number of air holes missing in the hexagonal lattice of the photonic crystal.
- A, where A is referring to the lattice constant of the photonic crystal.
- R0xx, where R0xx is referring to the diameter of the air holes in the photonic crystal.
- RM, where RM is referring to the relative diameter of the lateral edge air holes. For example RM80 means that the later edge air holes have a diameter which is 80% of the unmodified air holes.
- S0xx, where S0xx refers to the lateral displacement of the lateral edge holes. For example S018 means that the lateral air holes have moved 0.18A towards the edges respectively.

Fig. 3.3 shows a SEM image of a modified L3 cavity. As is visible in the figure the lateral edge holes have a reduced diameter and have moved to the lateral edge, indicating a modification in the RM and S0xx value.

3.3 Measurements

Before looking for evidence of lasing in the photonic crystal cavities, a characterization of the sample is performed. During these measurements the position of the fundamental mode of each cavity is determined in order to determine possible candidates for lasing. In this experiment, PCCs with a fundamental mode overlapping the ground state of the QDs have been considered.

As mentioned in section 2 there are several possible indicators whether a device is lasing or not. In order to obtain the L-L curves described in section 2.4.2 spectral measurements, varying the excitation laser power, have to be performed. For each value of the pump power a spectrum is taken. The spectrum of the cavity mode has a Lorentzian lineshape. By doing a Lorentzian fit the peak area as well as the linewidth can be determined.

In order to determine the carrier lifetime the setup described in 3.1.2 is used. Using the aforementioned setup, in combination with the PicoHarp 300 software, it is possible to create a histogram of the counts as a function of time. All the histograms in this report are made with a resolution of 32 ps. Using a fit which is similar to equation 5 it is possible to determine the carrier lifetime τ as function of power. This could present evidence of a possible lasing threshold as the carrier lifetime shows a different power dependence in lasing devices compared to nonlasing devices.

4 Characterization of the devices

In this section, the fundamental modes are characterized as a function of the modification of the PCC designs. This gives an indication as to how the fundamental mode position changes when changing certain parameters as well as the Q factor. The data of the parameter sweep can be found in Table D. It was observed that the fundamental mode position is largely influence by the lattice constant and the hole radius. The cavity modifications, the reduced radius and lateral movement of the edge holes, do not seem to influence the mode positions to a large extent, however these parameters may have a large influence on the Q factor of the cavities as mentioned in Section 2.2. This influence is illustrated in the difference in Q factor of the unmodified and modified L3 cavities (Table 4.1). Fig. 4.1 shows an example of a Lorentzian fit on the fundamental modes of the unmodified and modified L3 cavities.

The cavities which will be investigated for the lasing operation in the upcoming sections are:

- L3 A330 R028 RM100 S000 (unmodified)
- L3 A330 R028 RM80 S018 (modified)
- L7 A330 R028 RM80 S018 (modified)
- L11 A330 R028 RM80 S018 (modified)

As described in Section 2.2 the amount of missing air holes (3/7/11) determine the amount of cavity modes and changing the shape of the lateral edge air holes changes the position of the modes and the Q factor. The spectra are given in Appendix B. As the L7 and L11 cavities both have an additional mode (the second mode) in the QD emission range, this mode will be investigated as well for lasing.
The spectral position and Q factor of the modes which investigated in this report are given in table 4.1.

Table 4.1: *Data on the spectral positions and the Q factors of the investigated cavity modes. The Q factors for the unmodified L3 and modified L3/7/11 are obtained at 0.6 μW, 0.6 μW, 0.9 μW and 2.1 μW respectively.*

	Unmodified L3	***Modified L3***	***Modified L7***	**Modified L11**
Fundamental mode				
Wavelength (nm)	1231.00 ± 0.01	1239.69 ± 0.01	1249.31 ± 0.01	1247.18 ± 0.01
Q factor	2814.36 ± 133.86	5503.67 ± 167.58	9019 ± 747.579	9421.89 ± 731.15
Second mode				
Wavelength (nm)	-	-	1240.06 ± 0.01	1244.38 ± 0.01
Q factor	-	-	6805.77 ± 87.61	7732.59 ± 307.10

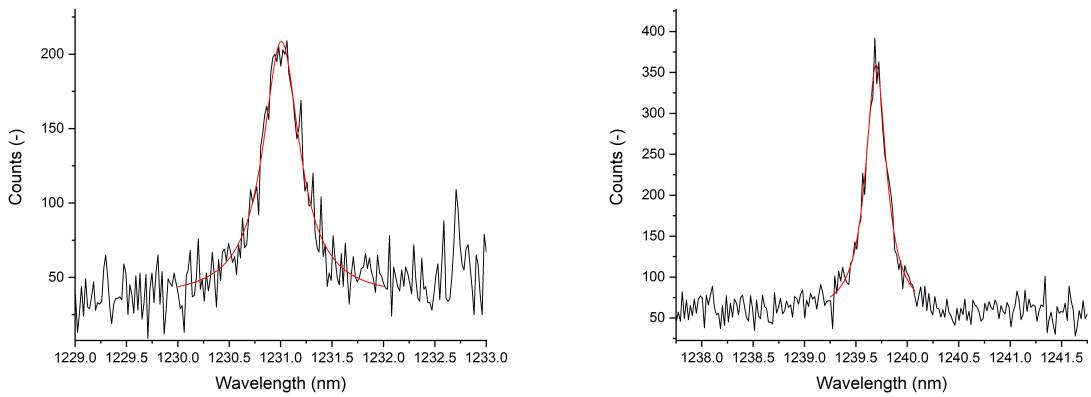

(a) **(b)**

Figure 4.1: *(a) Fundamental mode of the unmodified L3 cavity (black line), a Lorentzian fit was done the data (red line). (b) Fundamental mode of the modified L3 cavity (black line), a Lorentzian fit was done the data (red line). The Q factors are 2814.36 ± 133.86 and 5503.67 ± 167.58 respectively*

5 L-L & FWHM

5.1 L3 cavity

The first cavity investigated for lasing is the L3 cavity. The characterization study showed that the modified L3 cavity is a lasing candidate due to its high Q factor, and therfore low loss. Furthermore the cavity mode is in overlap with the QDs ground state which increases the gain. An unmodified L3 cavity is also investigated. This cavity is unlikely to be lasing due to its lower Q factor. The comparison between the modified and unmodified cavity should illustrate the differences between a cavity which is possibly lasing and a cavity which is not lasing.

A common indication of lasing is the presence of a kink in the L-L curve. As mentioned in Section 2.4.2 the magnitude of this kink is dependent on β. Since the L3 cavity only has one mode in the emission range of the QD's the β of the L3 cavity should be close to unity. Emission into the leaky modes and/or emission into other modes can decrease the β factor. The kink in the L-L curve in a high β laser can be difficult to observe, and therefore is insufficient to prove a lasing operation.

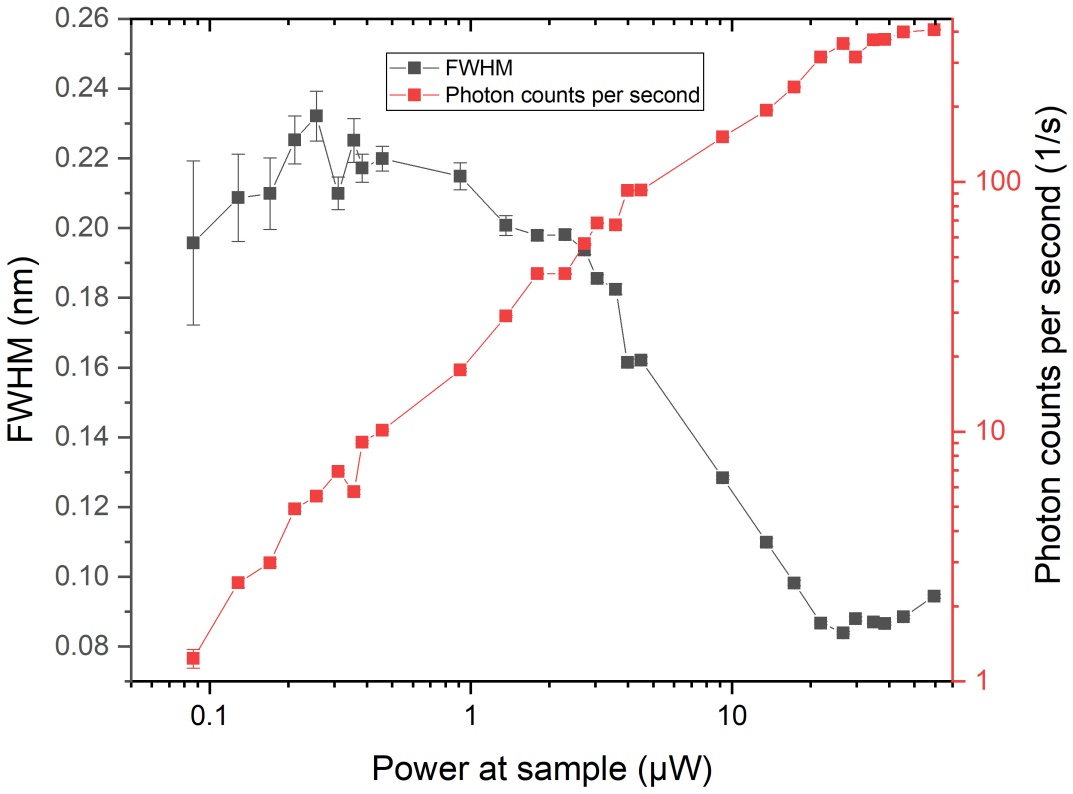

Figure 5.1: *Peak area per second of the modified L3 cavity(red squares). FWHM of the cavity mode(grey squares).*

Figure 5.1(red squares) shows a L-L curve of the modified L3 cavity with the measured FWHM(grey squares) as overlap. As mentioned above the kink in such a L-L curve is hard to observe. There is not a clear point where the output power shows nonlinear behavior. Since the used excitation power range includes the threshold values reported in previous works[37], this measurement suggests that if the PCC is lasing, it has a high β. The L-L curve also shows a decrease in slope at high pump power. Therefore it is not possible to conclude whether the cavity is lasing or not solely from the L-L curve. However, the threshold region where the kink should take place has another characteristic.
Using the same fit used to extract the peak area it is possible to extract the FWHM to investigate the linewidth narrowing. The linewidth narrowing of the modified L3 is also shown in Fig. 5.1(grey

squares). The linewidth shows a similar behavior as described in 2.4.2. At low excitation power, the FWHM shows a slight increase from its initial value of 0.195 to 0.232 nm. Then, the FWHM decreases until the excitation power reaches 1150 nW. Between 1.3 µW and 2.7 µnW the FWHM remains constant, and at higher power it decreases to 0.08 nm resulting in a reduction of factor 2.9. The presence of a plateau is the FWHM signature of the lasing operation as described in Section 2.4.2.

It is illustrative to compare the results of the modified cavity to the unmodified cavity to see whether the plateauing can be attributed to lasing or to some other mechanism. The unmodified design of the L3 has a fundamental mode with a Q-factor significantly lower(see Section 4) than the modified one.

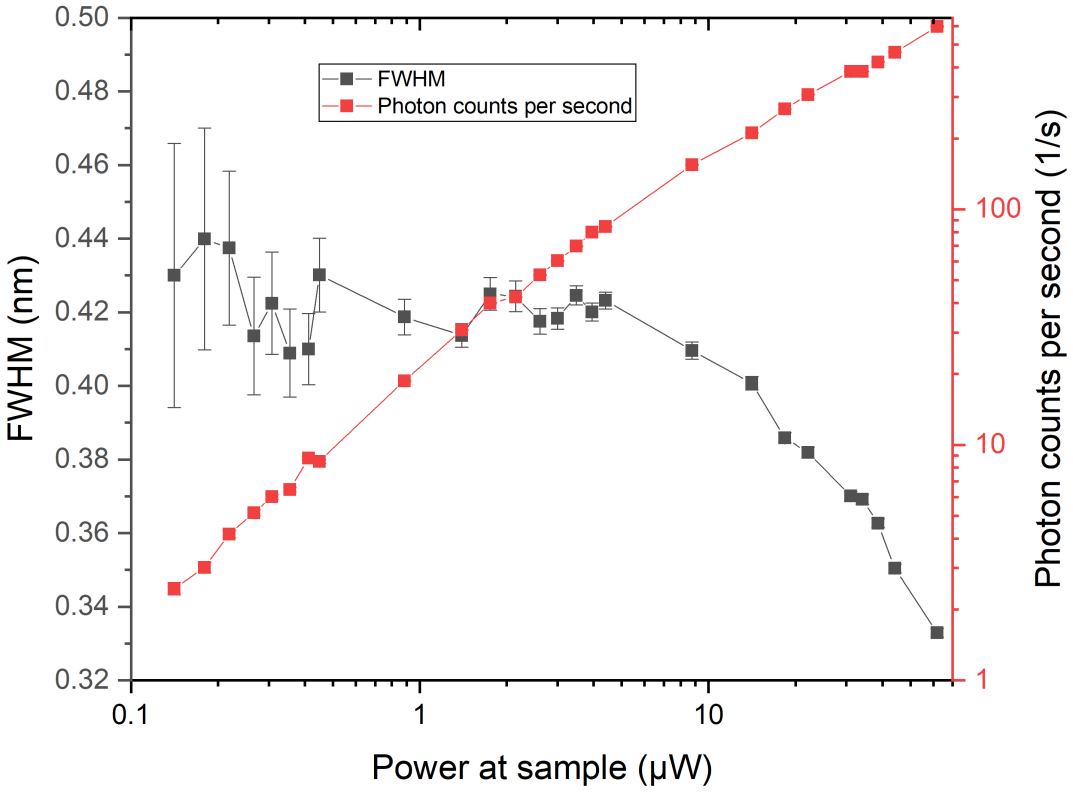

Figure 5.2: *Peak area per second of the unmodified L3 cavity(red squares). FWHM of the cavity mode(grey squares).*

Similar to the modified L3, the L-L curve from the unmodified L3 does not show any nonlinear behavior above a certain threshold as depicted in Figure 5.2. The behavior of the modified L3 FWHM is different from a modified L3. The behavior of slight narrowing followed by a plateau followed by drastic narrowing is much less pronounced, if not absent in Figure 5.2. The FWHM stays relatively constant up to 4.4 µW after which it starts to decrease at higher powers. The FWHM only decreased by a factor of 1.33 in contrast to the factor 2.9 with the modified cavity. This behavior is more similar to the standard Schawlow-Townes linewidth narrowing below threshold, where the cavity losses are constant, but the cavity mode experiences an increase in gain[28].

5.2 L7 cavity

Next the modified L7 cavity is investigated for lasing. The L7 cavity has more cavity modes than the L3 cavity due to its higher mode volume. Two of the cavity modes lie well within the emission range of the QDs, which are the fundamental and second mode as shown in Appendix B.2a. Therefore not only the fundamental mode is investigated, but the second mode as well.

5.2.1 fundamental mode

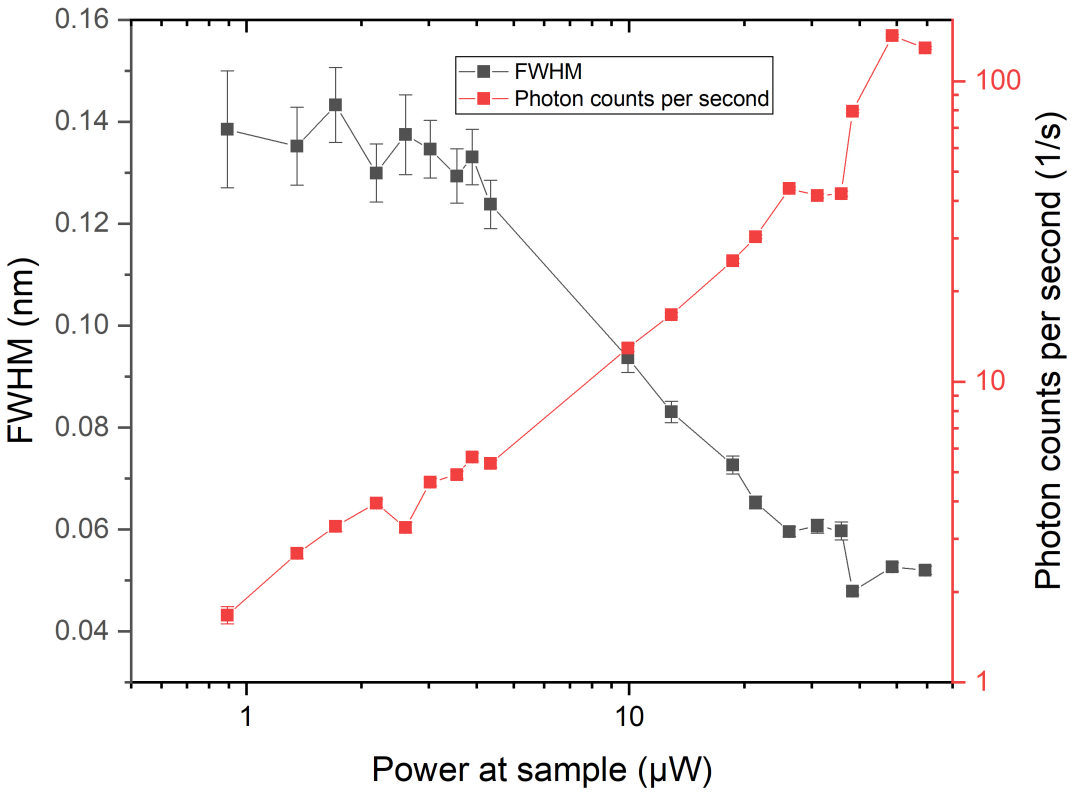

Figure 5.3: *Peak area per second of the modified L7 cavity(red squares). FWHM of the cavity mode(grey squares).*

At low pump power, the L-L curve shows a linear increase in the output power (Fig. 5.3(red squares)). A kink presents itself between 35.8 µW and 38.3 µW, indicating a possible lasing threshold. This kink is accompanied by a plateau like feature in the FWHM curve indicating that this is indeed a possible lasing threshold. The FWHM underwent a reduction of factor 2.99 from low to high power. Plotting the L-L curve in linear axes could provide a better indication of a kink in the curve.

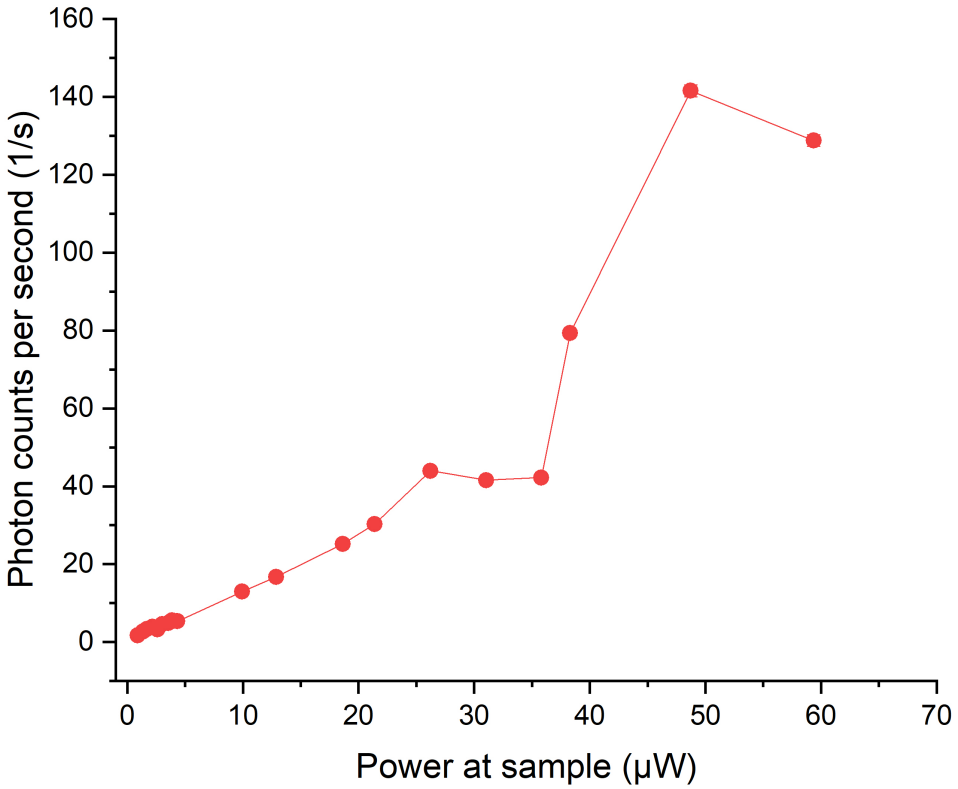

Figure 5.4: *Linear plot of the L-L curve of the fundamental mode of the modified L7. A kink is clearly present at 35.8 μW.*

Indeed, the L-L curve in linear axes (5.4) shows a clear change in slope after 35.8 μW.

5.2.2 Second mode

As mentioned, besides the fundamental mode, the second cavity mode of the modified L7 cavity is investigated as well.

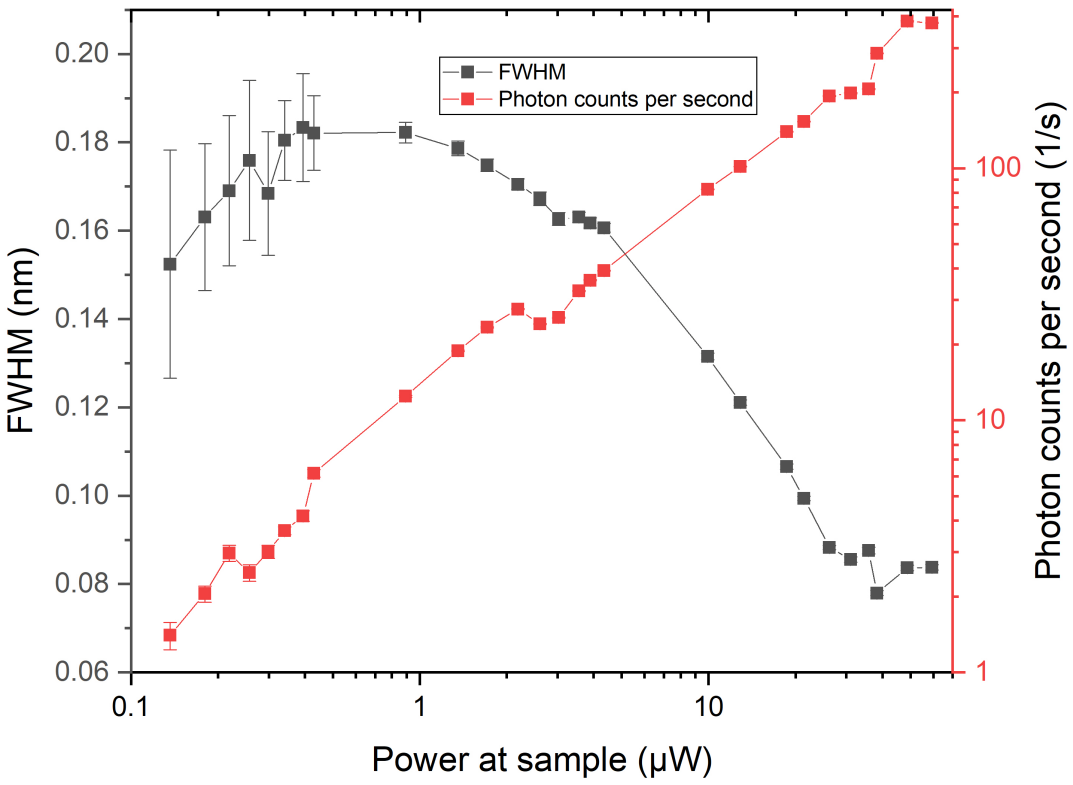

Figure 5.5: *Peak area per second of the modified L7 cavity(red squares). FWHM of the cavity mode(grey squares).*

Fig. 5.5 shows the L-L curve and the FWHM as function of power. Similarly as the fundamental mode, the L-L curve shows a kink-like feature around 35.8 µW, although less pronounced compared to the fundamental mode. The FWHM also shows some plateau-like feature at the same pump level, but just as the kink in the output power it is less pronounced. The FWHM underwent a reduction of factor 1.96 which is less than the reduction of the fundamental mode.
It is easier to examine the L-L when plotted in linear axes (5.6). The behavior of the L-L upward from 35.8 µW does show a nonlinear behavior. However when taking account the overall trend over the entire pump power range, the nonlinear behavior becomes more difficult to see as the slope in the low power regime is not that different from the slope in the high power regime. The increase of the output power is much less in this case. There is a 50% increase, instead of the doubling of output power in the case of the fundamental mode. At high power the output power starts to decrease, similar to the fundamental mode.

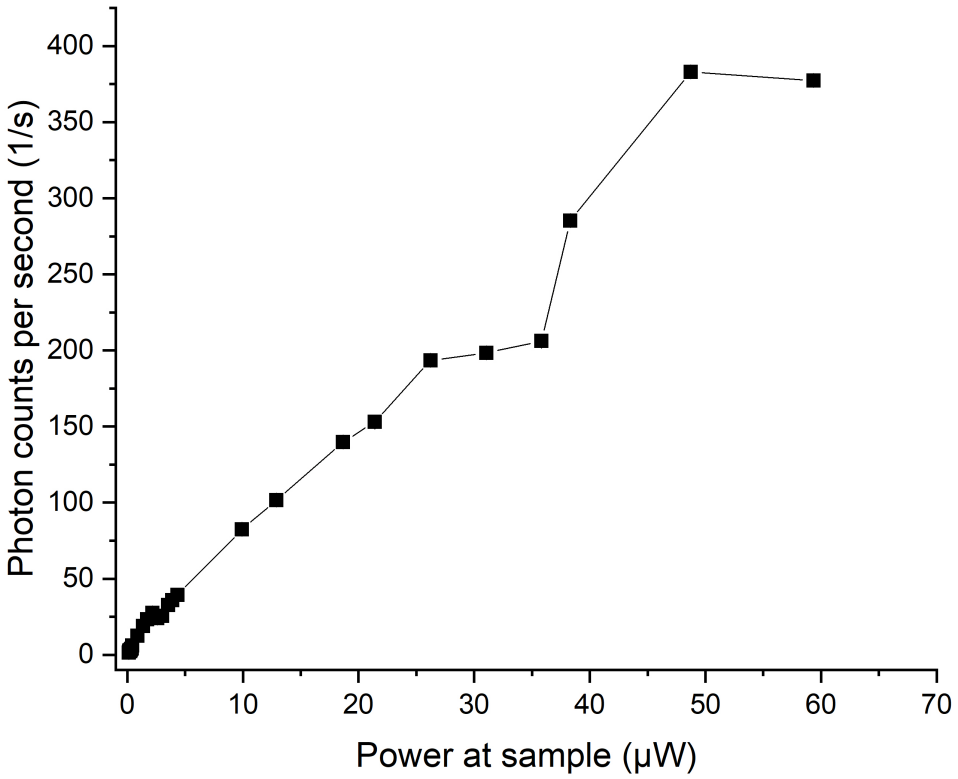

Figure 5.6: *Linear plot of the L-L curve of the fundamental mode of the modified L7. A kink-like feature is present at 35.8 μW.*

5.3 L11 cavity

Finally the fundamental and the second mode of the L11 cavity are investigated. As is the case with the L7, both modes overlap the ground state of the QDs as is shown Appendix B.2b.

5.3.1 Fundamental mode

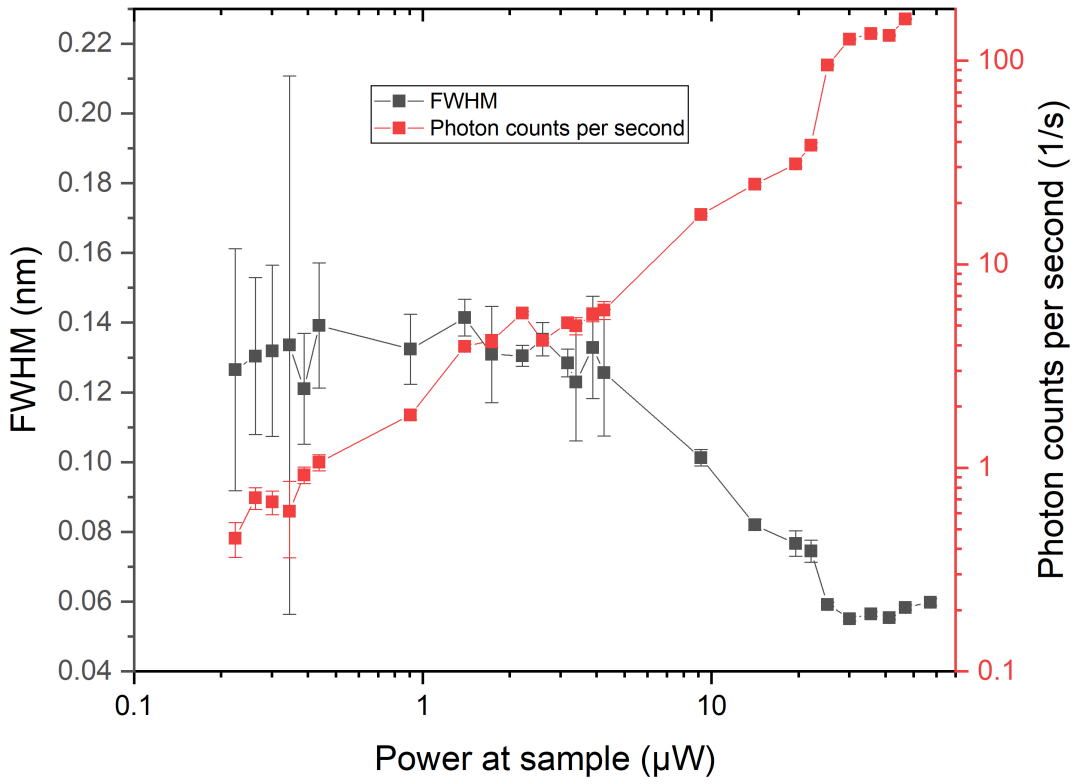

Figure 5.7: *(red squares)Peak area per second of the modified L11 cavity.(grey squares) FWHM of the cavity mode.*

The L-L of the L11 cavity fundamental mode shows a clear kink around 22.1 µW as is shown in Fig. 5.7. This kink is accompanied by a plateau in the FWHM trace of the same cavity, indicating that this cavity is lasing and that the threshold is around 22.1 µW. The FWHM undergoes a reduction, from low to high excitation power, of 2.30.

Fig. 5.8 clearly shows an increase in the output power of over 2 times between 22.1 µW and 25.2 µW. This suggests that the nanocavity is undergoing a transition into the stimulated emission regime at that point.

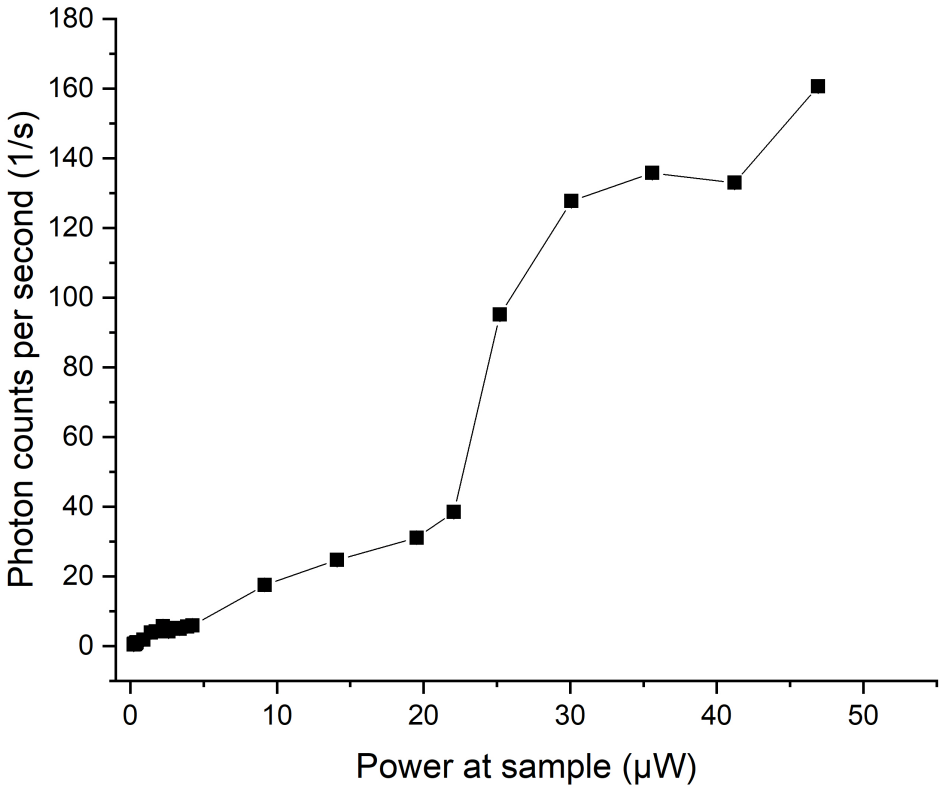

Figure 5.8: *Linear plot of the L-L curve of the fundamental mode of the modified L11. A kink is clearly present at 18.6 μW.*

5.3.2 Second mode

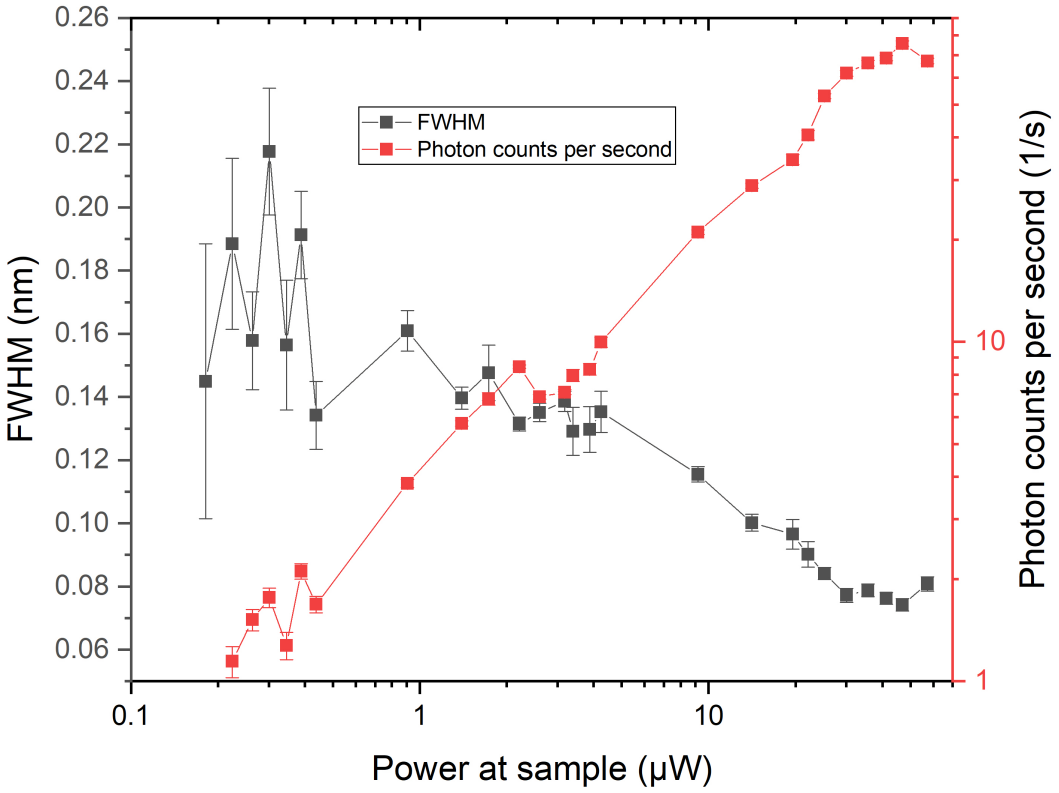

Figure 5.9: *(red squares)Peak area per second of the modified L11 cavity.(grey squares) FWHM of the cavity mode.*

While there is a kink-like feature present around 19.5 µW, as shown in Fig. 5.9 in the case of the second mode of the cavity, there does not seem to be such a clear kink in the L-L curve as with the fundamental mode. A plateau like feature is present around the same power, however there are not enough data points for it to be a convincing proof of lasing. The reduction of the FWHM from low to high power is a factor of 1.95. As was the case with the modified L7, the second mode has a lower reduction factor of the FWHM than the fundamental mode.

When plotted with linear axes, the L-L curve does show nonlinear behavior after 19.5 µW as shown in Fig. 5.10. This could be indicative of lasing as it is possible that both the fundamental and the second mode are lasing.

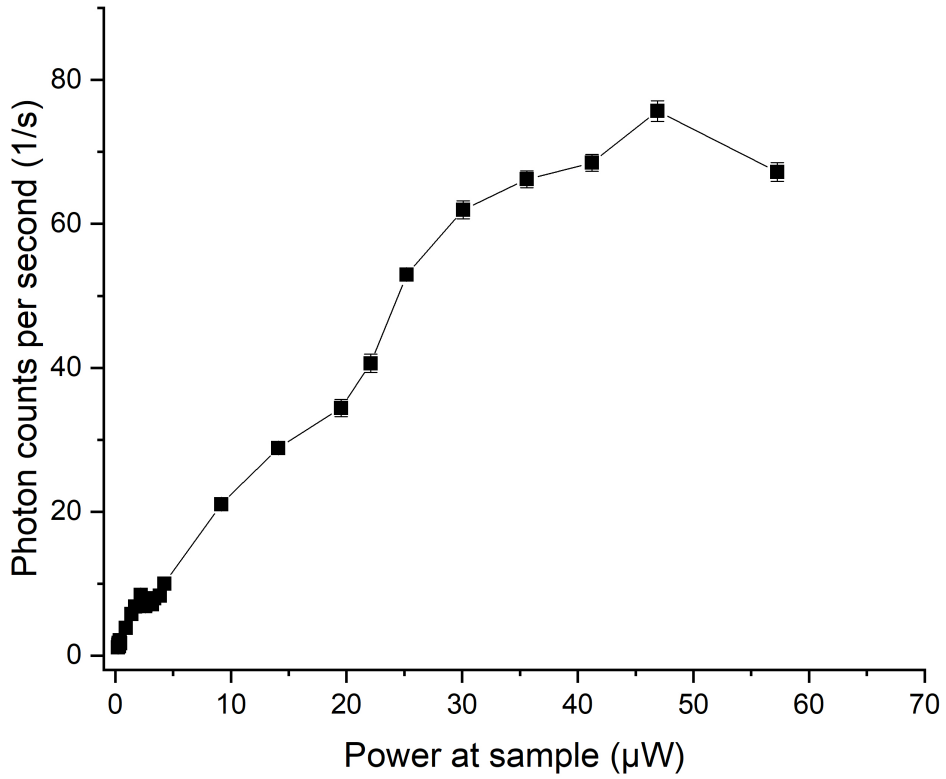

Figure 5.10: *Linear plot of the L-L curve of the fundamental mode of the modified L11. A kink-like feature is present at 19.5 μW.*

6 L-L vs. Background

In section 5 various L-L curves were investigated on superlinear behavior which is indicative of lasing. The L7 and L11 cavities both showed nonlinear behavior compatible with lasing, in contrast to both the modified and unnmodified L3 cavities which showed no such behavior.

The L-L curve of the modified L3 cavity obtained by a Lorentzian fit showed no nonlinearities. Therefore the L-L curve shown below is obtained by integration the QD emission 9.8 nm around the peak. Then the off resonant part of the QD spectrum, representing SE into the leaky modes is compared to the peak area obtained by a Lorentzian fit. This could provide insights on the relation between the output power of the cavity mode with regard to the off resonant spontaneous emission.

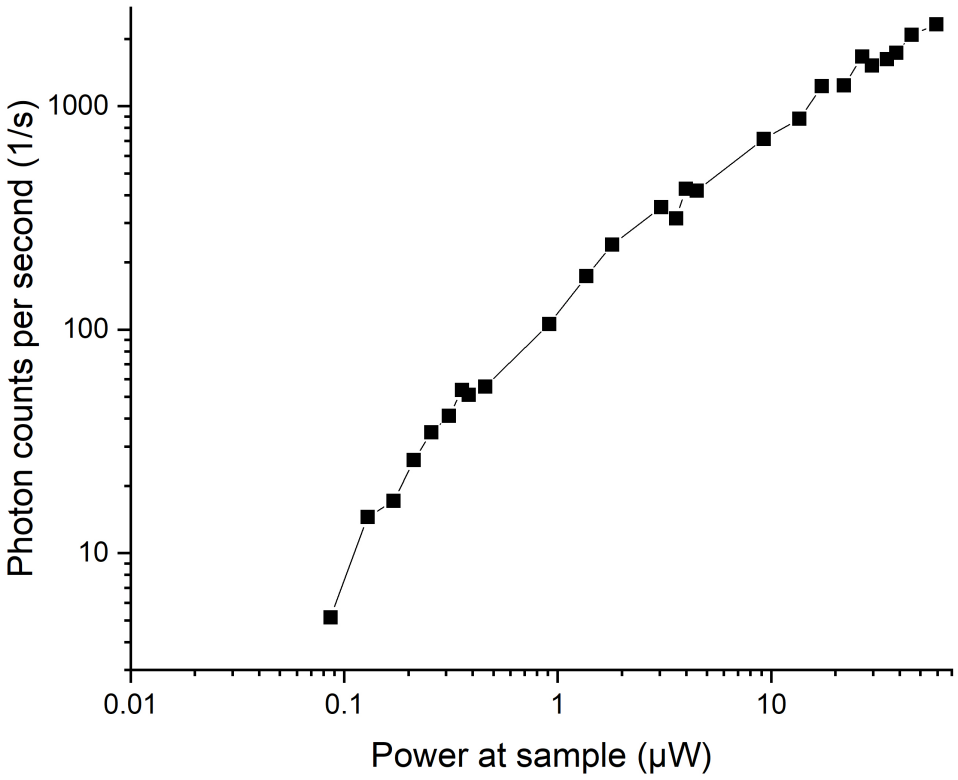

Figure 6.1: *Total area per second of the modified L3 spectra as function of power. The area was calculated using Origin. The spectral range over which was integrated is 9.8 nm.*

As shown in Fig. 6.1 there is not any kink-like feature in the L-L curve. This is the same behavior which the L-L of the modified L3 shows when only using the fit area. This indicates that the off resonant emission into the leaky modes scales linearly as well. To see whether this contribution truly scales linearly with power a L-L curve of the off resonant part of the spectrum was made.

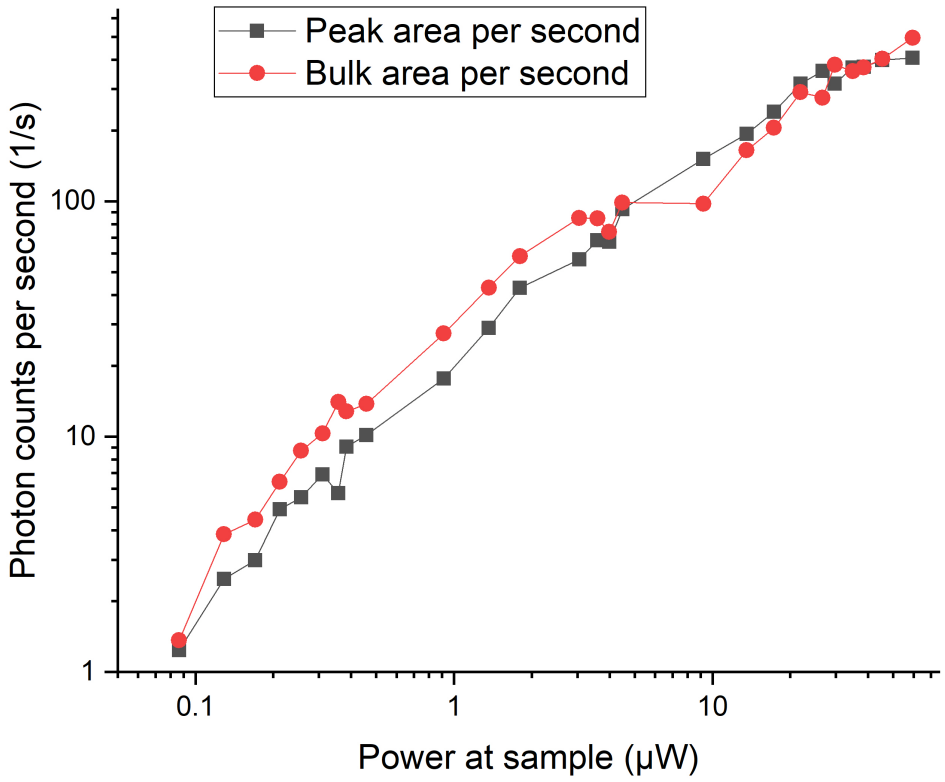

Figure 6.2: *Peak are per second of a modified L3, obtained using the fit area(squares). Off resonant area per second, obtained using a numerical fit over 2.5 nm in the off resonant part of the spectrum(circles).*

Fig. 6.2 illustrates the linear behavior of the leaky mode emission, confirming the suspicions that the off resonant contribution to the output power scales linearly. A linear fit on both L-L curves gave a slope of 0.79 ± 0.03 for the off resonant L-L and the cavity mode L-L has a slope of 0.88 ± 0.02.

7 Non-Lorentzian lineshape

During the course of the spectral measurements, an emission peak which showed a non-Lorentzian lineshape was observed, as is illustrated in Fig. 7.1. As is shown, near the maximum of the peak a feature is present which deviates from normal Lorentzian behavior.

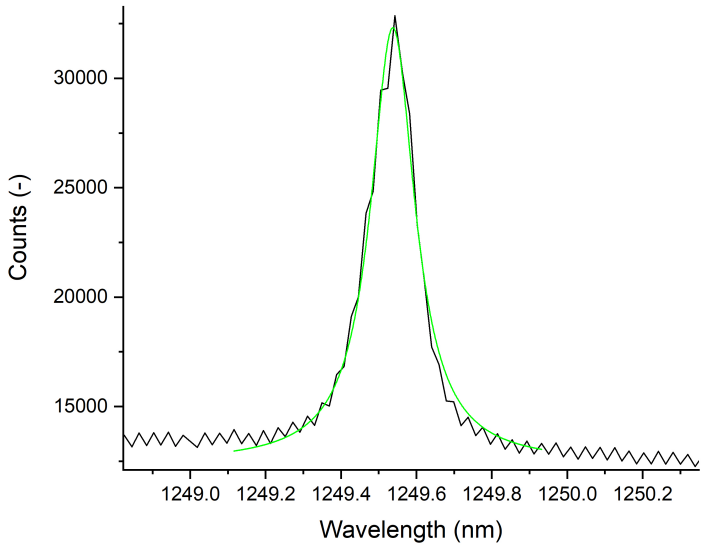

Figure 7.1: *(black line)The fundamental mode of the modified L7 cavity presenting a non Lorentzian lineshape.(green line) Best possible Lorentzian fit of the data .*

This non-Lorentzian lineshape presents a problem in the fitting of the experimental data as the fit can give a wrong estimation of the peak area and its FWHM.

First it was investigated whether this feature was due to some intensity related problem with the detector array of the spectrometer. However, the presence of this feature proves to be independent of the integration time as Fig. 7.2 depicts. Therefore it is unlikely that the presence this feature can be attributed to an intensity related issue in the InGaAs detector array of the spectrometer.
Since the µPL signal is integrated over a time period which is relatively long, this feature may suggest a fast switching of the cavity resonance in time. To further investigate this, time resolved measurements are needed.

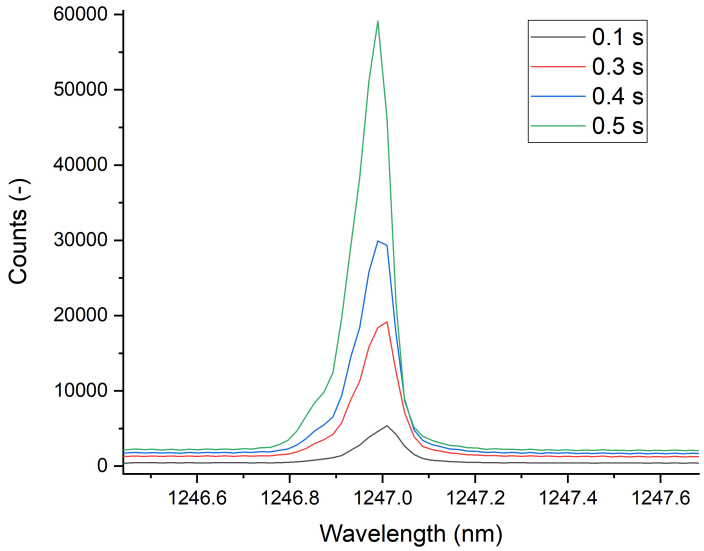

Figure 7.2: *A comparison of spectra belonging to the same cavity mode of the modified L7 cavity using different integration times. The spectra were obtained using an excitation power of 47.4 μW and a slit opening of 1 mm*

In order to resolve this issue, it was investigated whether the presence of this feature is dependent on the excitation power of the QDs. Fig. 7.3 illustrates the power dependence of the feature. Here it is shown that the non-Lorentzian feature is less present when using a lower excitation power as the fit is better in this case. A longer integration time was used to reduce a difference in total exposure on the detector array. However as for some measurements higher powers are required, making this an unfit solution to the problem. The power dependence on the present of this feature could have a relation to lasing as this feature was only reported in possible lasing cavities.

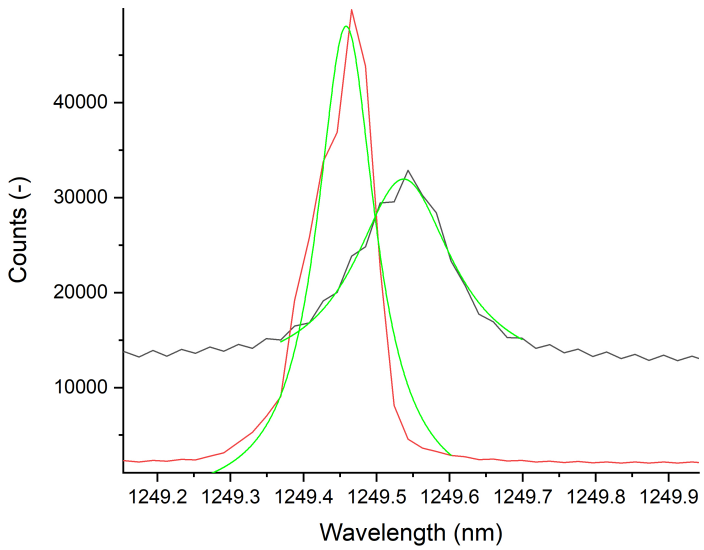

Figure 7.3: *(grey line) Spectrum of the fundamental mode of the modified L7 obtained by integrating for 10s with an excitation power of 4.15 μW. (red line) Spectrum of the same cavity mode obtained by integrating for 0.5s with an excitation power of 47.4 μW. The best possible fit of the modes (green lines)*

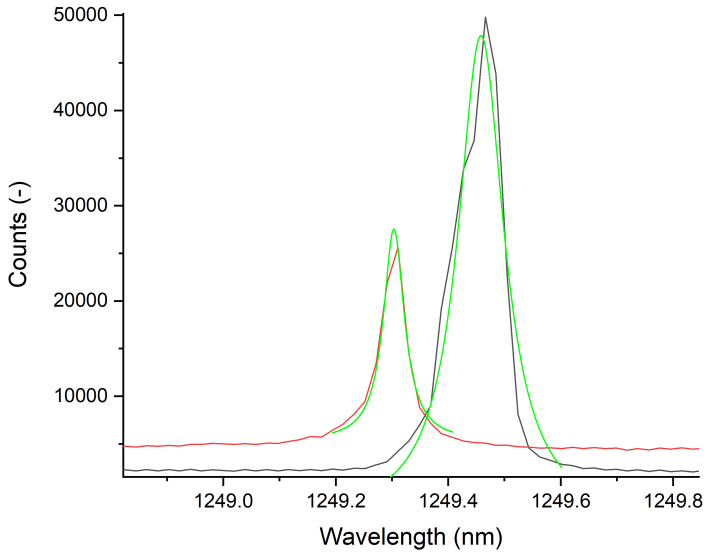

Figure 7.4: *(grey line) Cavity mode spectrum obtained by integrating 0.5 s with an excitation power of 47.4 μW using a slit opening of 1 mm. Cavity mode spectrum obtained by integrating 20 s with an excitation power of 47.4 μW using a slit opening of 0.6 mm.*

A different solution to resolve this issue is changing the opening slit of the spectrometer. The influence of changing the slit is shown in Fig. 7.4. Reducing the slit opening from 1 mm to 0.6 mm shows a cavity mode of a Lorentzian lineshape in the spectrometer. As reducing the slit width resolves this issue while allowing for high excitation powers, a reduced slit opening of 0.6 mm is used during the experiment.

8 Time resolved measurements

The cavities which were examined for lasing using spectral measurements, were also investigated using time resolved measurements to provide additional evidence for lasing. The measurement as described in Section 3.1.2 should provide insight as to how the carrier decay time behaves as a function of pump power. It is expected that non-lasing devices show poor power dependent decay time, while lasing devices display a bigger variation of the decay time due to the stimulated emission enhanced emission rate.

8.1 L3 cavity

In this section the time resolved measurements of the modified and unmodified L3 cavity modes are presented.

8.1.1 Modified L3 cavity

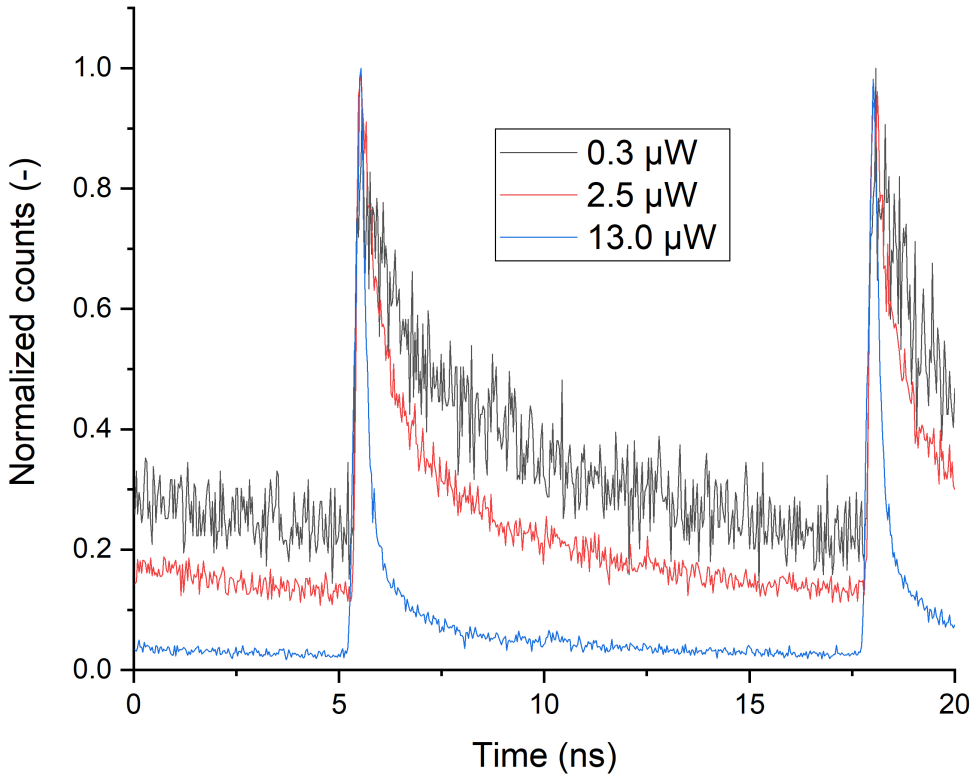

Figure 8.1: *Time resolved PL of the the modified L3 cavity. The counts (y-axis) are normalized.*

Fig. 8.1 shows the decay dynamics of the QDs at three different pump powers. A clear difference in decay times can be observed. This can be related to an enhanced emission rate into the cavity mode due to lasing as mentioned in 2.4.2. In order to determine the carrier lifetime an exponential fit of the data is performed. The fitting range in all cases is from the start of the decay (after the pump pulse) to 10 ns. This results in a fitting range of roughly 4.5 ns.

Until 0.43 µW the time resolved PL is well described by a mono exponential fit. Below this excitation power the decay time does not vary much and ranges between 1.43 ± 0.121 and 1.73 ± 0.179 ns as indicated by Fig. 8.2.

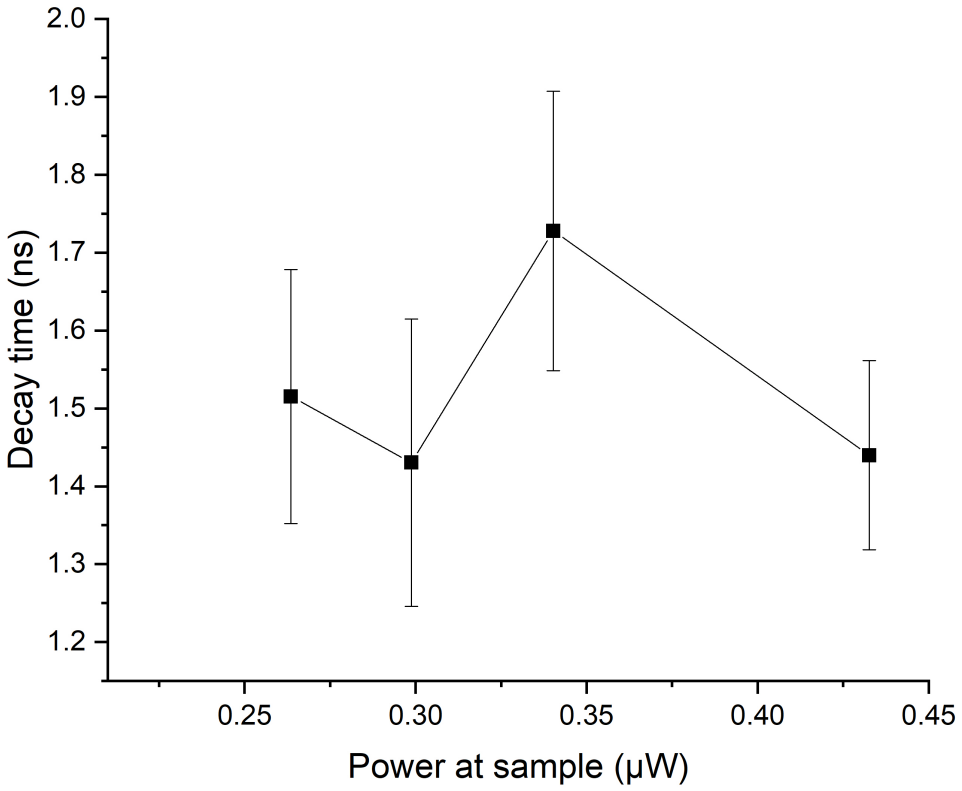

Figure 8.2: *Decay time obtained by a single exponential fit on a modified L3 cavity.*

However above 0.43 μW the mono exponential fit does not fit well anymore and a double exponential fit with a long and short decay time is required.

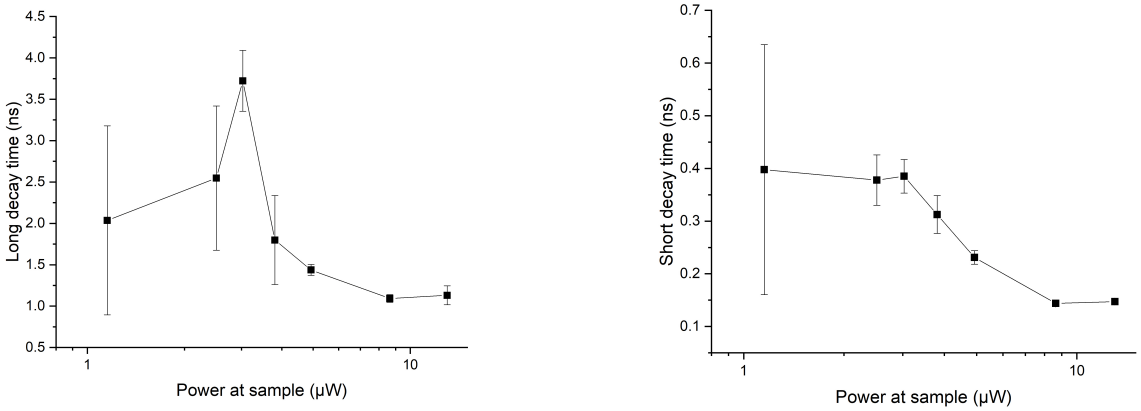

(a) **(b)**

Figure 8.3: *Long decay time obtained by a double exponential fit on the time resolved PL of the modified L3 as function of power(a). Short decay time (b).*

The short decay time varies from 0.40 ± 0.23 to 0.14 ± 0.01 ns. The decrease starts at 3.0 μW, indicating the presence of a possible lasing threshold. The long decay varies less with time and, varies from 2.0 ± 1.1 to 1.1 ± 0.1 ns. Furthermore the transition towards a double exponential was also observed by

Carnet-Ferret[39], this will further discussed in Section 9.

8.1.2 Unmodified L3 cavity

When comparing the time resolved PL from the modified L3 (Fig. 8.1) to the time resolved PL from the unmodified L3(Fig. 8.5), the difference in steepness of the decay is immediately visible. Unlike the

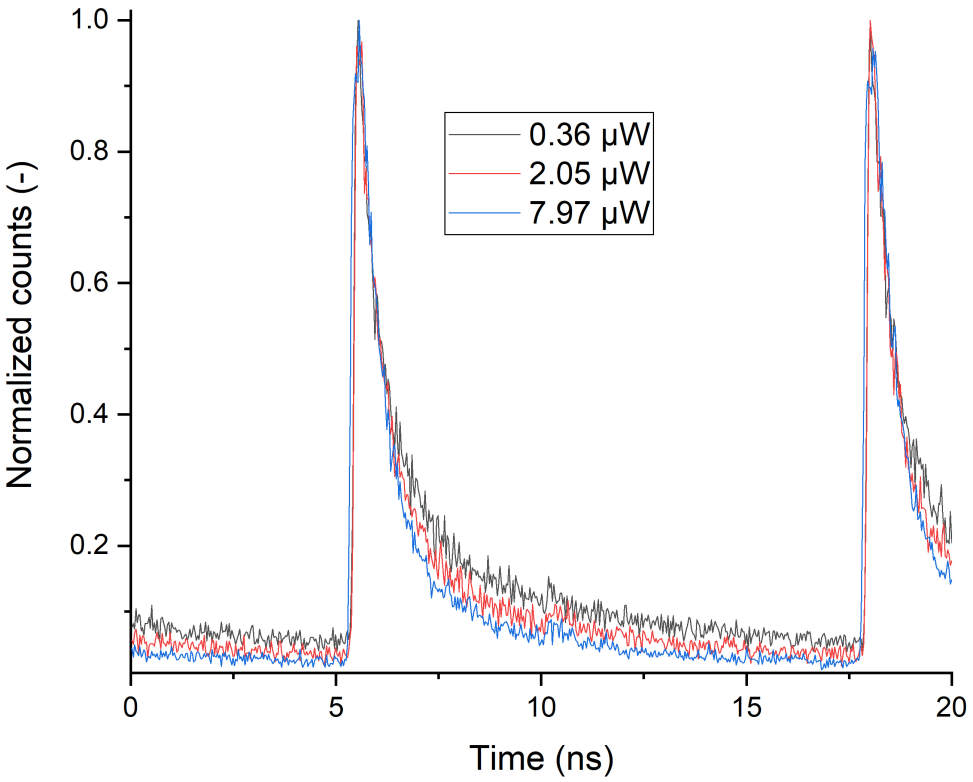

Figure 8.4: *Time resolved PL of the unmodified L3 cavity. Counts are normalized to one.*

modified L3, the unmodified L3 does not show an appreciable increase in steepness of the PL with power. To analyze the decay times a single exponential fit was used. Contrary to the modified L3, a double exponential fit is not required over the entire excitation power range.

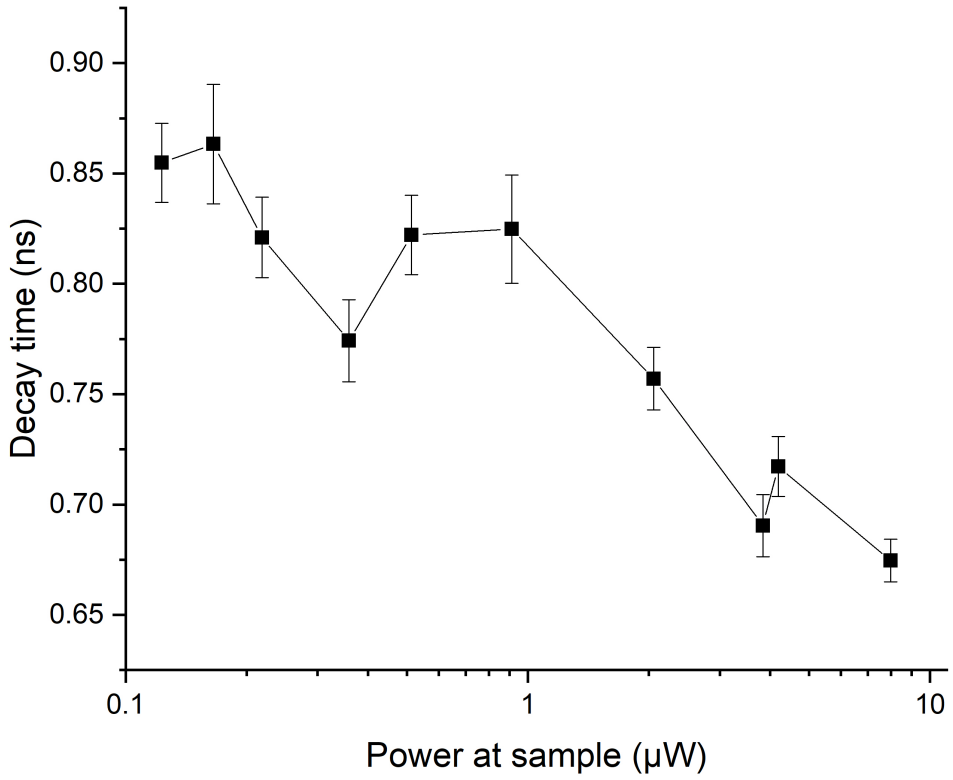

Figure 8.5: *Decay time obtained by a mono exponential fit on the time resolved PL of the unmodified L3 as function of power.*

Unlike the modified L3 cavity, the decrease of the decay time with increased excitation power, shown in Fig. 8.5 is limited, and is compatible to a non-lasing device due to its poor power dependency on the decay time[39]. Furthermore the non lasing device in5 did not present a double exponential decay, which is similar to this device.

8.2 L7 cavity

Just as the case with the L-L and FWHM, the first two modes of the L7 will be investigated.

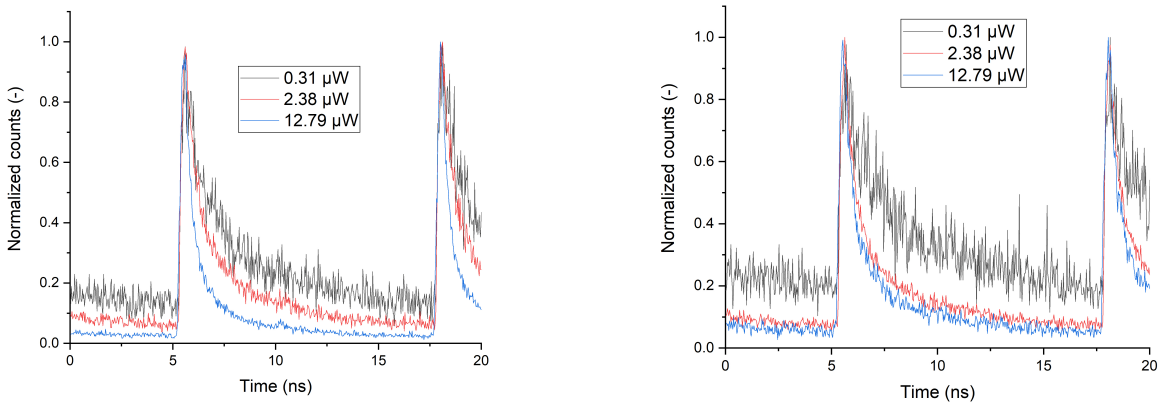

Figure 8.6: *Time resolved PL of the fundamental mode of the modified L3 cavity (a) and of the second mode (b). The counts are normalized.*

Both the fundamental mode and the second mode show a increase in steepness as power increases in the time resolved PL, illustrated by Fig 8.6. The decay of the fundamental mode is faster than the second mode, therefore displaying a higher emission rate than the second mode. As was the case with the modified L3 cavity, above 0.32 µW a mono exponential does not fit well anymore and a double exponential is required.

8.2.1 Fundamental mode

As the time resolved PL of the fundamental mode shows a faster decay at higher power in Fig. 8.6, a decrease in decay time is expected at higher excitation power.

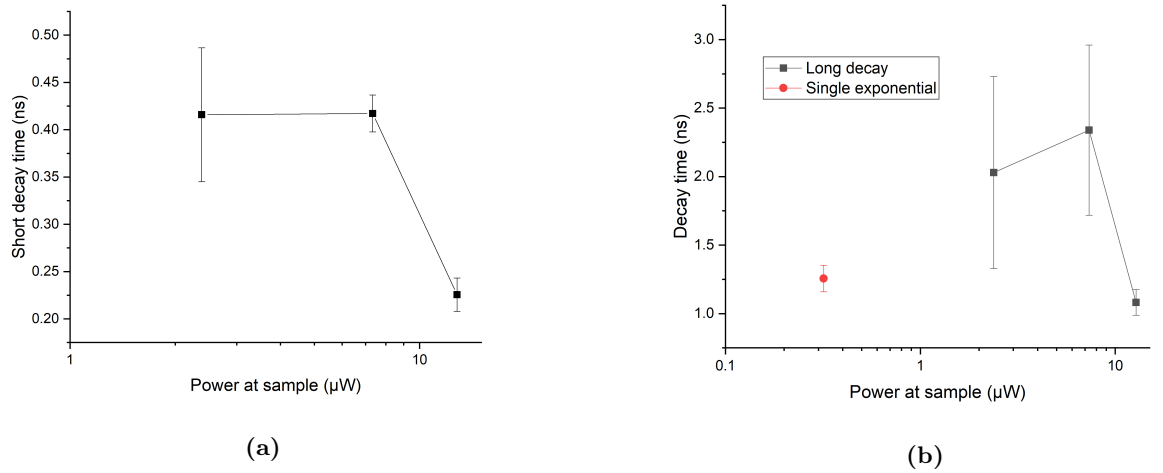

Figure 8.7: *(a)Short decay time obtained by a double exponential fit on the time resolved PL of the fundamental mode of the modified L7 as function of power.(b) Long decay time(squares) and the decay time obtained by a mono exponential fit at low power(circles) .*

The decay times obtained by the mono and double exponential fits are depicted in Fig. 8.7. The short decay time varies from 0.42 ± 0.07 to 0.22 ± 0.02 ns, and indeed as suspected the short decay time shows

a sudden decrease at 7.3 µW. The long decay time varies between 2.3 ± 0.7 and 1.1 ± 0.1 ns. The single exponential has a decay time of 1.3 ± 0.1.

8.2.2 Second mode

The time resolved PL of the second mode of the modified L7 cavity (Fig 8.6(b)) shows a faster decay time at higher pump power, similar to the fundamental mode.

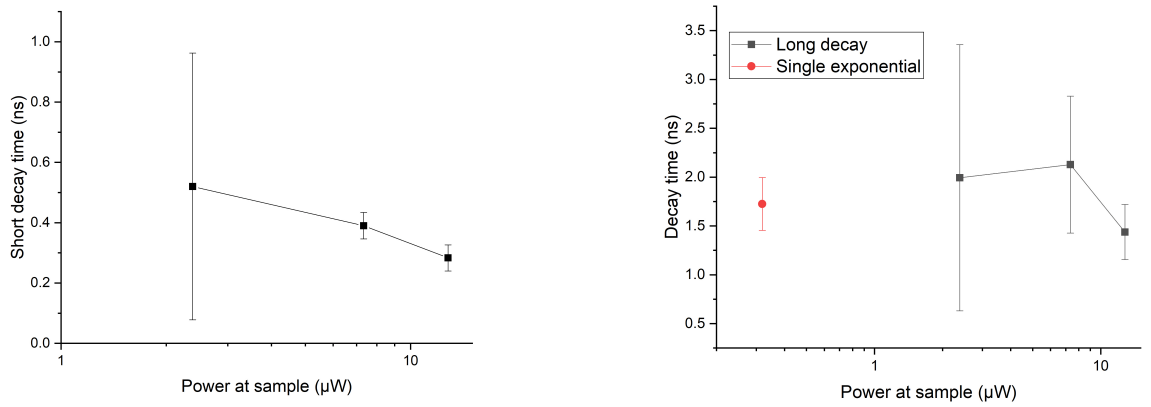

(a) **(b)**

Figure 8.8: *(a)Short decay time obtained by a double exponential fit on the time resolved PL of second mode of the modified L7 as function of power.(b)Long decay time(squares) and the decay time obtained by a mono exponential fit at low power(circles).*

The decay times obtained by the mono and double exponential fits are depicted in Fig. 8.7. The short decay time varies from 0.52 ± 0.44 to 0.28 ± 0.04 ns, and as suspected from Fig 8.6(b) the short decay time decreases as the pump power increases. The sudden decrease observed in the fundamental at 7.3 µW mode is less pronounced. The long decay time varies between 2.0 ± 2.0 and 1.4 ± 0.3 ns. The single exponential has a decay time of 1.7 ± 0.3 ns.

8.3 L11 cavity

Similar to the L7 cavity, two modes are investigated in the case of the L11 cavity. The fundamental and second mode.

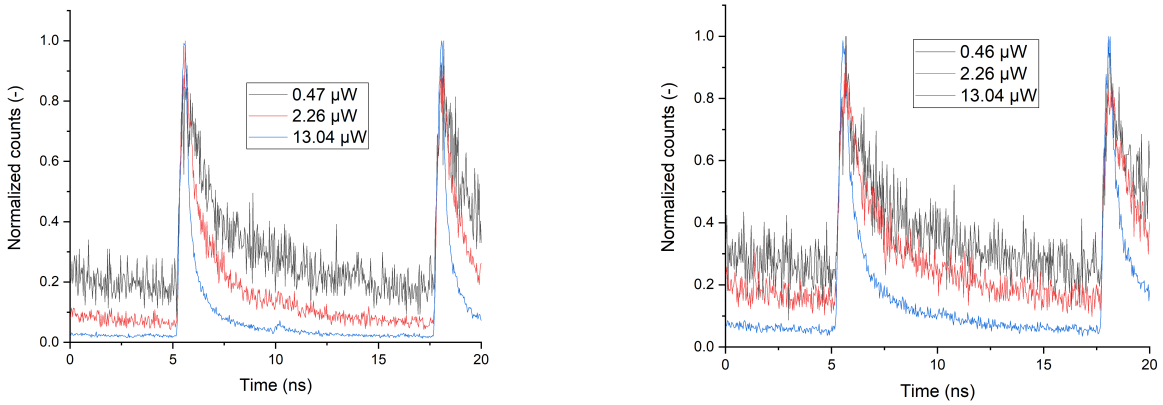

(a) **(b)**

Figure 8.9: *Time resolved PL of the fundamental mode of the modified L11 cavity (a) and the second mode (b). Counts are normalized to one.*

As is the case for the L7 cavity, the time resolved PL for both the fundamental and second mode (Fig. 8.9) shows a decrease in decay time. Similar to the L7 cavity, the time resolved PL shows that the fundamental mode has a higher emission rate than the second mode. At pump powers above 0.47 and 0.46 µW for the fundamental and second mode respectively a mono exponential fit does not fill well anymore and a double exponential fit is required.

8.3.1 Fundamental mode

From Fig. 8.9 it is expected that the fundamental mode shows a decrease in decay time at higher pump power.

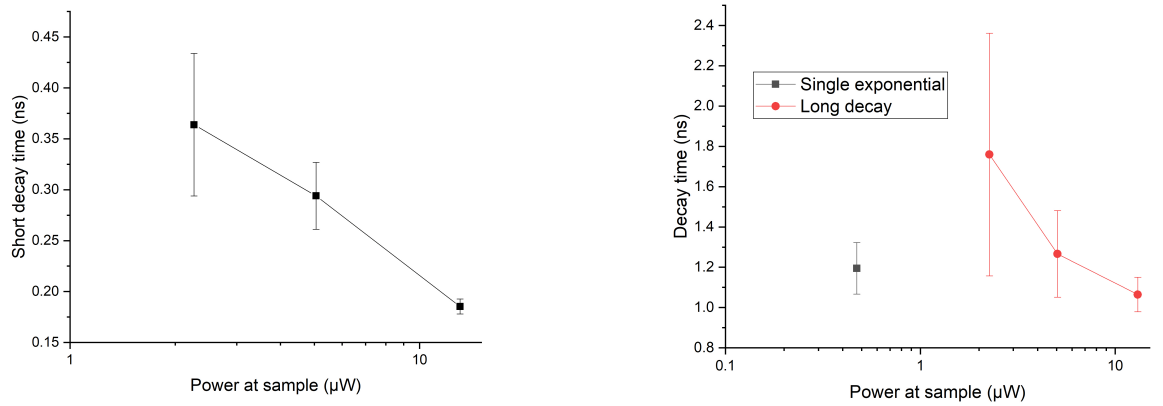

(a) **(b)**

Figure 8.10: *(a)Short decay time obtained by a double exponential fit on the time resolved PL of the fundamental mode of the modified L11 as function of power.(b) Long decay time(squares) and the decay time obtained by a mono exponential fit at low power(circles) .*

The decay times obtained by the mono and double exponential fits are shown in Fig. 8.10. Indeed as suspected from Fig. 8.9 the decay times do decrease with increasing pump power. The short decay time

varies from 0.36 ± 0.07 to 0.18 ± 0.01 ns. The short decay does not show a sudden decrease at a certain pump power, but rather a gradual decrease. The long decay time varies from 1.7 ± 0.6 to 1.1 ± 0.1 ns. The mono exponential fit provided a decay time of 1.2 ± 0.1 ns.

8.3.2 Second mode

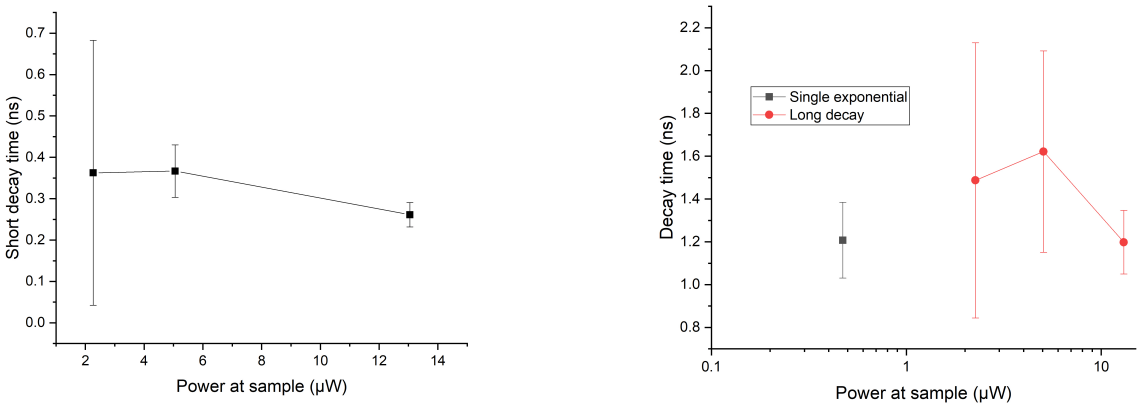

(a) **(b)**

Figure 8.11: *(a)Short decay time obtained by a double exponential fit on the time resolved PL of the second mode of the modified L11 as function of power.(b) Long decay time(squares) and the decay time obtained by a mono exponential fit at low power(circles) .*

The decay times obtained by the mono and double exponential fits are shown in Fig. 8.11. Similar to the fundamental mode, the decay times do decrease with increased pump power as suspected from Fig. 8.9. The short decay time varies from 0.36 ± 0.32 to 0.26 ± 0.03 ns. As is the case with the fundamental mode, the short decay times do not show a sudden decrease at a certain power, but rather a gradual decrease. The long decay time does not vary as much and varies from 1.6 ± 0.5 to 1.2 ± 0.1 ns. The mono exponential fit provided a decay time of 1.2 ± 0.1 ns.

9 Discussion

Most of the results presented at sections 4 to 8 are obtained by fitting experimental data. The errors in the produced results are obtained by the fitting error given by the software used (Origin). In general the fitting error can underestimate actual error. Doing multiple measurements per pump power should provide a better indication of the value (for example the decay time) obtained by the fit as taking the average of multiple values represents an alternative way to quantify errors with statistics.

A different issue related to the fiting presented itself when obtaining the FWHM and L-L values. At high enough powers (30 µW) the emission peaks become so narrow that only 3 to 4 data points per peak were available. This resolution (0.02 nm) limit reduces the reliability of the FWHM value obtained by the fit at high power. This is especially true for the L7 and L11 cavities as a possible lasing threshold presented itself around that power.

Another observation at high powers in the L-L curve is that the output power stops increasing and even sometimes decreases (for example see Fig 5.4). As this decrease is present in all L-L curves this is probably related to thermal effects of the increased pump power[28]. The low amount of data points in the spectrum could also contribute to this effect. In section 2.4.2 it was mentioned that a kink in a L-L curve could also possibly be attributed to a biexciton contribution at higher powers. However, in this case this seems unlikely as the kink in the L-L is accompanied with a plateau-like feature in the FWHM curve, indicating that the kink can be attributed to lasing.

Additionally the observation of a non-Lorentzian lineshape was made at sufficiently high powers7. This feature proved to be independent on the intensity on the detector array of the spectrometer, while a dependency on the excitation power was noted. This dependency on the excitation power could indicate that this feature is somehow related to lasing. Albeit, an additional study on this feature is required to make any further conclusions.

The observation of the transition of a mono exponential decay towards a double exponential decay in the time resolved PL was also observed by Canet-Ferrer in the case of a L7 cavity using quantum wires as gain medium[39]. There it is reported that the presence of a long decay time accompanied by a short decay time can be attributed to the existence of photon recycling processes. These processes were reported in H type PCC with InGaAsP quantum wells as gain medium[8]. A different explanation of the long decay could be the presence of poorly coupled QDs into the lasing mode of the cavity[40]. The long decay time could then possibly be attributed to the contribution of the QD emission into the leaky modes. A possible experiment to verify this, is a time resolved PL measurement of a photonic crystal with the same lattice constant and hole radius, but without any defects. This allows for the decay rate into the leaky modes to be quantified.

As can be seen from for example Fig. 8.10, the values obtained for the decay times of the cavities come with rather large fitting uncertainties. This is due to the comparatively low counts at the low power to high power. Some low power time resolved PL have a maximum count as low as 90 counts. To resolve this a new measurement with longer integration time is needed. Furthermore as mentioned above repeating the measurements for the same pump power should also provide more accurate results.

Lastly it is important to compare the results observed in the L-L curve, linewidth narrowing and time resolved measurements to conclude whether the cavities are lasing or not. The unmodified L3 cavity does not seem to be lasing from the L-L and FWHM(Fig. 5.2). The decay time obtained by the mono exponential fit also does not decrease any appreciable amount. Furthermore the unmodified L3 is the only cavity which only requires a mono exponential fit for all pump powers. The presence of a double exponential could possibly have some relation to lasing. However additional time resolved measurements on different cavities is required to make any further conclusions on the connection between lasing and the presence of a double exponential decay.
In contrast to the unmodified L3, the modified L3 does seem to show behavior characteristic of lasing. While the L-L of the L3 does not provide any evidence for lasing, the behavior of the FWHM as function of power is characteristic of lasing (Fig 5.1). As described in 2.4.2 the plateu region in the FWHM is indicative of a lasing threshold. This plateau ranges from 1.3 µW to 2.7 µW. The time resolved PL of the modified L3 has a mono exponential decay up to 0.43 µW. The short decay time of the double

exponential starts to decay at 3.0 µW. The data indicates that the cavity shows lasing behavior, and that the lasing threshold is present between 1.15 µW and 3.0 µW

In contrast to the L3 cavities the modified L7 cavity does show a kink in the L-L curve. The fundamental cavity mode exhibits a sharp increase in power at 35.8 µW (Fig.5.3). This sharp increase in power is accompanied by a plateau-like feature in the FWHM curve which ranges from 26.2 µW to 35.8 µW. However as mentioned above due to the resolution limit at such high pump power the FWHM may not be reliable. Unfortunately there is not a time resolved PL of the modified L7 at such high powers. However as described in [39], if the cavity is lasing, the carrier lifetime should decrease an appreciable amount before the lasing threshold. As shown in Fig. 8.7 there is a sudden decrease in decay time at 6.2 µW. Still, more measurements are required to conclude whether the fundamental mode is lasing or not from the time resolved measurements. Although, the L-L and the FWHM curve indicate that the fundamental mode of the modified L7 cavity is lasing and that the threshold lies somewhere between 26.2 µW and 35.8 µW
The second mode also has a kink-like feature in the L-L at 35.8 µW, however the kink is less pronounced as the kink in the fundamental mode. Furthermore the plateau-like feature which is present at the same pump power as the kink is less pronounced as in the fundamental mode. The plateau-like feature ranges from 26.2 µW to 35.8 µW. The time resolved PL behaves similarly as the fundamental mode. The data indicates that the second mode could be lasing. If the cavity is lasing a possible threshold would be ranging between 26.2 µW and 35.8 µW. However it is not conclusive if the cavity is lasing.

The fundamental mode of the L11 cavity shows a pronounced kink in the L-L curve. The power suddenly increases over two times above 22.1 µW (Fig.5.7). This increase is accompanied by a plateau like feature which ranges from 19.6 µW to 22.1 µW. The time resolved measurements show that the short decay time is gradually decreasing with pump power. As is the case with the L7 cavity, additional measurements with higher pump powers are required to draw a conclusion from the time resolved PL. However the kink in the L-L and the FWHM curve clearly indicate that the fundamental mode is lasing and that the threshold lies somewhere between 19.6 µW to 22.1 µW.
Just as the fundamental mode, the second mode has a kink like feature. The kink is present at 19.6 µW (5.9). However the kink is much less visible as with the fundamental mode. Furthermore the plateauing, ranging from 14.1 µW to 19.6 µW, is less pronounced. The short decay time behaves similarly as the fundamental mode. Concluding from the L-L and FWHM curve it is possible that the second mode is lasing and has a threshold between 14.1 µW to 19.6 µW, however additional measurements are required to draw a definite conclusion.

The significantly higher threshold powers of the L7 and L11 cavities than the L3 cavity could be explained by three factors. The first factor which can cause this is the higher mode volume of the cavity. Secondly the L7/11 modes lie further outside the ground state of the quantum dots than the fundamental mode of the L3 cavity causing a lower net gain of the cavity mode.

To draw definite conclusions whether the cavity modes of the modified L3/7/11 cavities are lasing a $g^{(2)}(0)$ is required. If the cavities are lasing the value of the $g^{(2)}(0)$ should make a transition from 2 to 1 as described in Section 2.4.2. Unfortunately due to problems with the setup it was not possible to measure the $g^{(2)}(0)$ within the given time constraints of the project. Therefore a $g^{(2)}(0)$ would be a good additional measurement to perform in the future. Furthermore an excitation laser which has a more stable power can help improve the clarity of the L-L curves, and possibly show slight nonlinearities which otherwise are hidden by systematic errors.

10 Conclusion

In conclusion, an experimental study on PCC using self assembled QDs as gain medium was performed. Several cavities were characterized and three cavities, the modified L3/7/11 cavities, were investigated for lasing. An unmodified L3 cavity was also investigated to function as baseline as this cavity was unlikely to be lasing due to its lower Q factor.
It is shown that the L-L curves of modified L7/11 cavities show behavior which is characteristic of lasing. The linear behavior of the modified L3 L-L curve is inconclusive for lasing. The FWHM curves of all three modified cavity show a plateau like feature which is characteristic of lasing in nanostructures. The time resolved PL of the modified cavities shows a double exponential behavior which is possibly related to lasing. The short decay times of the modified cavities show a decrease as function of power, however the time resolved PL measurements do not present definitive evidence supporting lasing operation. The second modes of the modified cavities show behavior similar to the fundamental modes, however, less pronounced. Additionally, the unmodified L3 cavity showed no behavior characteristic of lasing which is in line with expectations. Furthermore, during the study a lineshape with a non-Lorentzian feature presented itself at lasing conditions. This feature could have a relation to lasing, however this requires further investigation.
The reported lasing thresholds of the fundamental cavity modes are between 1.3µW to 3.0 µW, 26.2 µW to 35.8µW and 19.6µW to 22.1µW for the modified L3/7/11 cavities respectively, which order of magnitude is compatible with other works[36][37]

References

[1] A. Baroni, A. De Filippis, G. Oliviero, A. Fusco, B. Perfetto, E. Buommino, and G. Donnarumma. Effect of 1064-nm q-switched nd:yag laser on invasiveness and innate immune response in keratinocytes infected with candida albicans. *Lasers in Medical Science*, 33(5):941–948, 2018. ISSN: 1435-604X. DOI: 10.1007/s10103-017-2407-3. URL: https://doi.org/10.1007/s10103-017-2407-3.

[2] B. Mukherjee. *Optical communication networks*, volume 14. McGraw-Hill New York, 1997.

[3] S. R. Forrest, M. R. Gokhale, F. Xia, and V. Menon. Photonic integrated circuits, 2004. US Patent 6,795,622.

[4] Gaas integrated quantum photonics: towards compact and multi-functional quantum photonic integrated circuits. English. *Laser and Photonics Review*, 10(6):870–894, Nov. 2016. ISSN: 1863-8880. DOI: 10.1002/lpor.201500321.

[5] J. M. Gérard, B. Sermage, B. Gayral, B. Legrand, E. Costard, and V. Thierry-Mieg. Enhanced spontaneous emission by quantum boxes in a monolithic optical microcavity. *Phys. Rev. Lett.*, 81:1110–1113, 5, 1998. DOI: 10.1103/PhysRevLett.81.1110. URL: https://link.aps.org/doi/10.1103/PhysRevLett.81.1110.

[6] D. Englund, D. Fattal, E. Waks, G. Solomon, B. Zhang, T. Nakaoka, Y. Arakawa, Y. Yamamoto, familyi=c., given=Jelena, giveni=J., ,, and. Controlling the spontaneous emission rate of single quantum dots in a two-dimensional photonic crystal. *Phys. Rev. Lett.*, 95:013904, 1, 2005. DOI: 10.1103/PhysRevLett.95.013904. URL: https://link.aps.org/doi/10.1103/PhysRevLett.95.013904.

[7] T. J. Kippenberg, S. M. Spillane, and K. J. Vahala. Demonstration of ultra-high-q small mode volume toroid microcavities on a chip. *Applied Physics Letters*, 85(25):6113–6115, 2004. DOI: 10.1063/1.1833556. eprint: https://doi.org/10.1063/1.1833556. URL: https://doi.org/10.1063/1.1833556.

[8] K. Nozaki, S. Kita, and T. Baba. Room temperature continuous wave operation and controlled spontaneous emission in ultrasmall photonic crystal nanolaser. *Opt. Express*, 15(12):7506–7514, 2007. DOI: 10.1364/OE.15.007506. URL: http://www.opticsexpress.org/abstract.cfm?URI=oe-15-12-7506.

[9] P Gogna, M Loncar, T Yoshie, A Scherer, and Y Qiu. Low-threshold photonic crystal laser, 2002.

[10] S. Strauf, K. Hennessy, M. T. Rakher, Y.-S. Choi, A. Badolato, L. C. Andreani, E. L. Hu, P. M. Petroff, and D. Bouwmeester. Self-tuned quantum dot gain in photonic crystal lasers. *Phys. Rev. Lett.*, 96:127404, 12, 2006. DOI: 10.1103/PhysRevLett.96.127404. URL: https://link.aps.org/doi/10.1103/PhysRevLett.96.127404.

[11] H. Altug, D. Englund, and J. Vuckovic. Ultrafast photonic crystal nanocavity laser. *Nature Physics*, 2:484 EP –, 2006. URL: http://dx.doi.org/10.1038/nphys343. Article.

[12] T. Asano, W. Kunishi, B.-S. Song, and S. Noda. Time-domain response of point-defect cavities in two-dimensional photonic crystal slabs using picosecond light pulse. *Applied Physics Letters*, 88(15):151102, 2006. DOI: 10.1063/1.2194010. eprint: https://doi.org/10.1063/1.2194010. URL: https://doi.org/10.1063/1.2194010.

[13] Y. Chu, Y. Yang, X. Hu, Z. Chen, Y. Ma, Y. Liu, Y. Wang, L. Liao, Y. Xing, H. Li, J. Peng, N. Dai, J. Li, and L. Yang. Yb3+ heavily doped photonic crystal fiber lasers prepared by the glass phase-separation technology. *Opt. Express*, 25(20):24061–24067, 2017. DOI: 10.1364/OE.25.024061. URL: http://www.opticsexpress.org/abstract.cfm?URI=oe-25-20-24061.

[14] T. Sato, K. Takeda, A. Shinya, M. Notomi, K. Hasebe, T. Kakitsuka, and S. Matsuo. Photonic crystal lasers for chip-to-chip and on-chip optical interconnects. *IEEE Journal of Selected Topics in Quantum Electronics*, 21(6):728–737, 2015. ISSN: 1077-260X.

[15] A. Bahabady, S. Olyaee, and H. Arman. Optical biochemical sensor using photonic crystal nanoring resonators for detection of protein concentration. 13:1–1, Apr. 2017.

[16] E. Knill, R. Laflamme, and G. J. Milburn. A scheme for efficient quantum computation with linear optics. *Nature*, 409:46 EP –, 2001. URL: http://dx.doi.org/10.1038/35051009. Article.

[17] D. Pellegrino, F. Pagliano, A. Genco, M. Petruzzella, F. W. v. Otten, and A. Fiore. Deterministic control of radiative processes by shaping the mode field. *Applied Physics Letters*, 112(16):161110, 2018. DOI: 10.1063/1.5026803. eprint: https://doi.org/10.1063/1.5026803. URL: https://doi.org/10.1063/1.5026803.

[18] G. Kim, J. W. Park, I. G. Kim, S. Kim, S. Kim, J. M. Lee, G. S. Park, J. Joo, K.-S. Jang, J. H. Oh, et al. Low-voltage high-performance silicon photonic devices and photonic integrated circuits operating up to 30 gb/s. *Optics express*, 19(27):26936–26947, 2011.

[19] J. Joannopoulos. *Photonic Crystals: Molding the Flow of Light*. Princeton University Press, 2008, pages 17–18. ISBN: 978-0691124568.

[20] S A. H. Nekuee, M. Akbari, and K. Mehrany. A novel method for band structure analysis of photonic crystal slabs. 3:1111–1122, Dec. 2011.

[21] S. Noda, A. Chutinan, and M. Imada. Trapping and emission of photons by a single defect in a photonic bandgap structure. *Nature*, 407:608 EP –, 2000. URL: http://dx.doi.org/10.1038/35036532.

[22] Q. Dot and P. N. group. Quality factor of si-based photonic crystal l3 nanocavities probed with an internal source. URL: http://www.qdgroup.u-psud.fr/photonics.html (visited on 06/24/2018).

[23] Y. Akahane, T. Asano, B.-S. Song, and S. Noda. High-q photonic nanocavity in a two-dimensional photonic crystal. *Nature*, 425:944 EP –, 2003. URL: http://dx.doi.org/10.1038/nature02063.

[24] Y. Xu, K. Meehan, L Guido, G. Lu, C. L. Wyatt, and N. G. Love. Synthesis and characterization of silica coated cdse/cds core/shell quantum dots, Dec. 2005.

[25] W. Ouerghui, A. Melliti, M. Maaref, and J. Bloch. Dependence on temperature of homogeneous broadening of ingaas/inas/gaas quantum dot fundamental transitions. *Physica E: Low-dimensional Systems and Nanostructures*, 28(4):519 –524, 2005. ISSN: 1386-9477. DOI: https://doi.org/10.1016/j.physe.2005.05.051. URL: http://www.sciencedirect.com/science/article/pii/S1386947705002158.

[26] L. N. Bimberg D. G. M. *Quantum Dot Heterostructures*. 1999. ISBN: 978-0-471-97388-1.

[27] J. A. Vernables. *Introduction to Surface and Thin Film Processes*. Camebridge University Press. ISBN: 0 521 62460 6.

[28] S. W.M. L. Coldren L. *Diode Lasers and Photonic Integrated Circuits*. Wiley.

[29] B. Romeira and A. Fiore. Purcell effect in the stimulated and spontaneous emission rates of nanoscale semiconductor lasers. *IEEE Journal of Quantum Electronics*, 54(2):1–12, 2018. ISSN: 0018-9197. DOI: 10.1109/JQE.2018.2802464.

[30] H. Yokoyama and S. D. Brorson. Rate equation analysis of microcavity lasers. *Journal of Applied Physics*, 66(10):4801–4805, 1989. DOI: 10.1063/1.343793.

[31] C. Gies, J. Wiersig, M. Lorke, and F. Jahnke. Semiconductor model for quantum-dot-based microcavity lasers. *Phys. Rev. A*, 75:013803, 1, 2007. DOI: 10.1103/PhysRevA.75.013803. URL: https://link.aps.org/doi/10.1103/PhysRevA.75.013803.

[32] S. M. Ulrich, C. Gies, S. Ates, J. Wiersig, S. Reitzenstein, C. Hofmann, A. Löffler, A. Forchel, F. Jahnke, and P. Michler. Photon statistics of semiconductor microcavity lasers. *Phys. Rev. Lett.*, 98:043906, 4, 2007. DOI: 10.1103/PhysRevLett.98.043906. URL: https://link.aps.org/doi/10.1103/PhysRevLett.98.043906.

[33] S. Ritter, P. Gartner, C. Gies, and F. Jahnke. Emission properties and photon statistics of a single quantum dot laser. *Opt. Express*, 18(10):9909–9921, 2010. DOI: 10.1364/OE.18.009909.

[34] A. L. Schawlow and C. H. Townes. Infrared and optical masers. *Phys. Rev.*, 112:1940–1949, 6, 1958. DOI: 10.1103/PhysRev.112.1940. URL: https://link.aps.org/doi/10.1103/PhysRev.112.1940.

[35] U. Mohideen, R. E. Slusher, F. Jahnke, and S. W. Koch. Semiconductor microlaser linewidths. *Phys. Rev. Lett.*, 73:1785–1788, 13, 1994. DOI: 10.1103/PhysRevLett.73.1785. URL: https://link.aps.org/doi/10.1103/PhysRevLett.73.1785.

[36] G. Björk, A. Karlsson, and Y. Yamamoto. On the linewidth of microcavity lasers. *Applied Physics Letters*, 60(3):304–306, 1992. DOI: 10.1063/1.106693.

[37] S. Strauf, K. Hennessy, M. T. Rakher, Y.-S. Choi, A. Badolato, L. C. Andreani, E. L. Hu, P. M. Petroff, and D. Bouwmeester. Self-tuned quantum dot gain in photonic crystal lasers. *Phys. Rev. Lett.*, 96:127404, 12, 2006. DOI: 10.1103/PhysRevLett.96.127404. URL: https://link.aps.org/doi/10.1103/PhysRevLett.96.127404.

[38] S. W.M. L. Coldren L. *Diode Lasers and Photonic Integrated Circuits*. Wiley, pages 59–62.

[39] J. Canet-Ferrer, I. Prieto, G. Muñoz-Matutano, L. J. Martínez, L. E. Muñoz-Camuniez, J. M. Llorens, D. Fuster, B. Alén, Y. González, L. González, P. A. Postigo, and J. P. Martínez-Pastor. Excitation power dependence of the purcell effect in photonic crystal microcavity lasers with quantum wires. *Applied Physics Letters*, 102(20):201105, 2013. DOI: 10.1063/1.4807439.

[40] J. Canet-Ferrer and L. J. M. nez. Purcell effect in photonic crystal microcavities embedding inas/inp quantum wires. *Opt. Express*, 20(7):7901–7914, 2012. DOI: 10.1364/OE.20.007901.

Appendices

Appendix A. Laser rate equations

The way the gain, the pump and the optical resonator interact with each other can be described by the laser rate equations. The laser rate equations are two coupled differential equations, an equation for the carrier generation rate(6 and an equation for the photon generation rate (10). The carrier rate equation describes the carrier density variation in the active region of the laser. The active region is the region where recombining carriers contribute tot useful gain and photon emission. In the active region the behavior can be desribed by a generation term, which is due to the pump power, and multiple recombination processes which can be radiative or nonradiative. Thus the carrier rate equation can be written as:

$$\frac{dn}{dt} = G_{gen} - R_{rec} = \frac{\eta_i I}{qV} - R_{rec} \tag{6}$$

where n is the carrier density[1], G_{gen} is the carrier generation rate, R_{rec} is the carrier recombination rate per unit volume in the active region, I is the injected current, η_i is the carrier injection efficiency, q is the carrier charge and V is the active region volume. The recombination process consist out of multiple mechanisms. It consists out of a spontaneous recombination rate R_{SE}, a nonradiative recombination rate, R_{NR}, a stimulated emission rate R_{ST} and if necessary a leaky carrier rate R_L can be included. Thus R_{rec} can be written as

$$R_{rec} = R_{SE} + R_{NR} + R_{ST} + R_L \tag{7}$$

The third term, the stimulated emission requires the presence of photons. It is common to describe the natural decay processes, meaning an absence of photons and generation term, by a carrier lifetime τ. This gives

$$\frac{dn}{dt} = -\frac{n}{\tau} = R_{SE} + R_{NR} + R_L \tag{8}$$

Using this fact the carrier recombination rate can be written as

$$\frac{dn}{dt} = \frac{\eta_i I}{qV} - R_{rec} - \frac{n}{\tau} - R_{ST}. \tag{9}$$

The photon rate equation for a single optical mode in the active region can be described similarly by generation terms and a loss term. The photon density equation has the following form:

$$\frac{dn_\phi}{dt} = \Gamma R_{ST} + \beta\Gamma R_{SE} - \frac{n_\phi}{\tau_\phi} \tag{10}$$

where n_ϕ is the photon density[2], Γ the confinement factor, β the spontaneous emission (SE) rate into the lasing mode divided by the total SE rate, and τ_ϕ the photon lifetime.

[1] Note: in some literature N is used as carrier density.
[2] Note: in some literature N_ϕ is used as photon density.

Appendix B. Cavity spectra

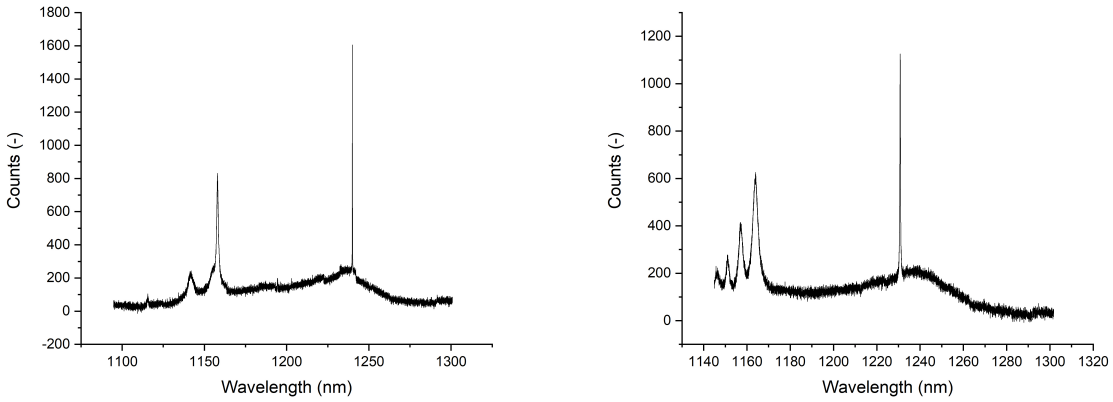

(a) **(b)**

Figure B.1: *(a) Spectrum of the modified L3 cavity. (b) Spectrum of the unmodified L3 cavity.*

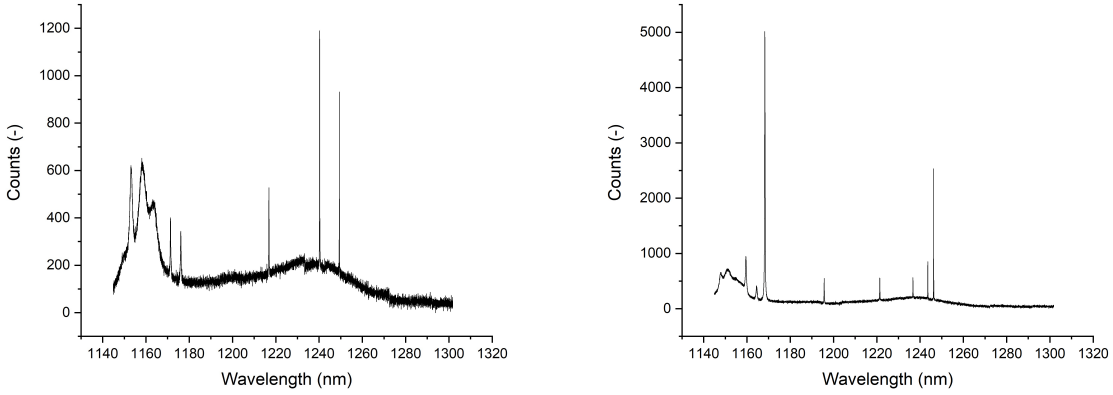

(a) **(b)**

Figure B.2: *(a) Spectrum of the modified L7 cavity. (b) Spectrum of the modified L11 cavity.*

Appendix C. QD emission spectrum

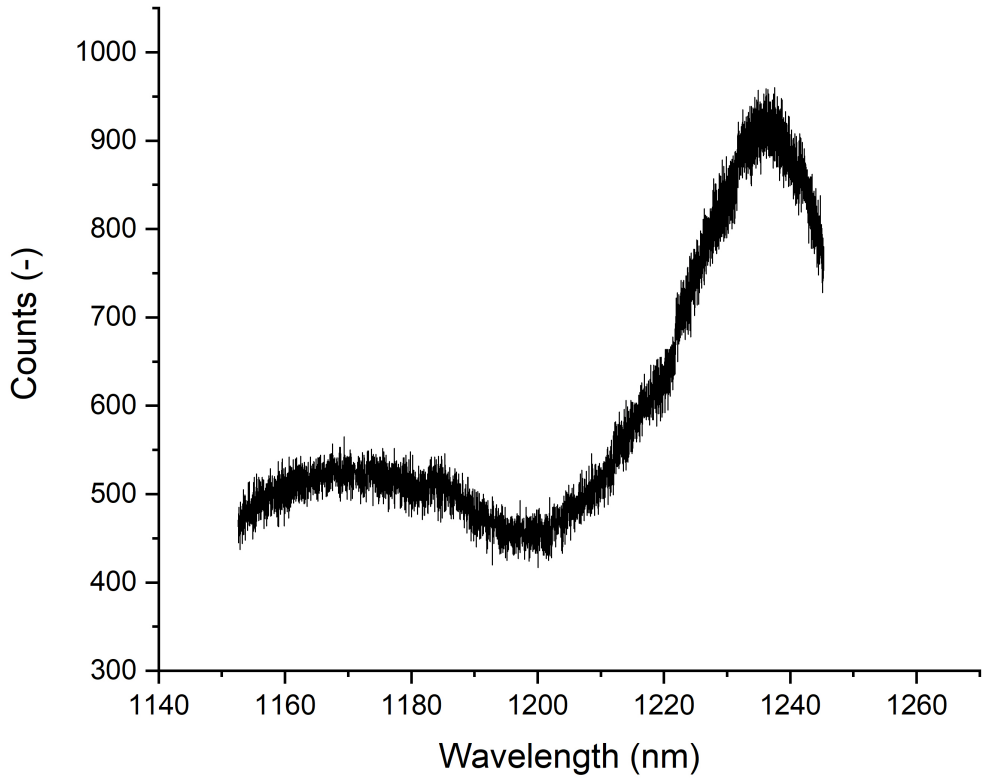

Figure C.1: *Emission spectrum of the QDs at 77 K.*

Appendix D. Fundamental modes position

Table D.1: *Spectral position of the fundamental modes of several PCCs.*

RM variation	Fundamental mode (nm)
L3 A330 R029 S00	
RM100	1223,78
RM80	1228,24
L7 A330 R029 S00	
RM100	1239,77
RM80	1243,24
RM70	1243,43
L11 A330 R029 S00	
RM100	1243,14
RM80	1243,54
RM70	1245,29

S0xx variation	Fundamental mode (nm)
L3 A330 R029 RM100	
S00	1223,78
S018	1233,4
L7 A330 R029 RM100	
S00	1239,77
S018	1241,05
S019	1242,83
L11 A330 R029 RM100	
S00	1243,14
S018	1244,6
S019	1244,82

R0xx variation	Fundamental mode (nm)
L3 A330 RM100 S00	
R028	1231,95
R029	1223,78
L7 A330 RM100 S00	
R028	1248,9
R029	1239,77
L11 A330 RM100 S00	
R028	1248,4
R029	1243,14

A variation	Fundamental mode (nm)
L3 R028 RM100 S00	
A330	1248,9
A340	1274,49
A350	1291,86
L7 R028 RM100 S00	
A330	1248,4
A340	1279,9
A350	1294,64
L11 R028 RM100 S00	
A330	1231,95
A340	1258,95
A350	1287,77